OBSERVATIONS ON THE MOBILIZATION OF STRENGTH IN REINFORCED SOIL STRUCTURES

by

VICENTE SANTIAGO QUINTEROS

B.Eng. University of Applied Sciences Rapperswil, Switzerland, 2008

A THESIS SUBMITTED IN PARTIAL FULFILLMENT OF
THE REQUIREMENTS FOR THE DEGREE OF

MASTER OF APPLIED SCIENCE

in

THE FACULTY OF GRADUATE AND POSTDOCTORAL STUDIES
(Civil Engineering)

THE UNIVERSITY OF BRITISH COLUMBIA
(Vancouver)

October 2014

© Vicente Santiago Quinteros, 2014

ABSTRACT

Confidence in the design of reinforced retaining structures is based on a limited body of experimental field data from performance monitoring of a relatively small number of case studies. In order to improve upon that confidence in design, this research addresses the back-analysis of the only field study involving a reinforced steep slope with independent measurements of tensile force and strain, which was first described by Fannin & Hermann (1990). Knowing the mobilized strength in the reinforcement, a back-analysis was performed using widely accepted design practice, with the purpose of establishing the mobilized angle of friction within the backfill soil of the structure. The mobilized friction angle was compared with the findings of laboratory shear strength tests in direct shear, triaxial and plane-strain conditions. The comparison provides further evidence in support of the expectation that plane-strain conditions prevail within the reinforced steep slope, and the recommendation in the British code of practice to use the peak friction angle for design. Additionally, visual inspection and index testing on exhumed geogrid samples from the structure described by Fannin & Hermann (1990) established that the geogrid has experienced no major physical damage, nor any significant degradation associated with durability of the polymer material. Moreover, rapid loading creep tests data show excellent agreement between exhumed and typical values, implying no significant durability degradation in the geogrid of the Skedsmo structure. Accordingly, isochronous load-strain-time data can be used with confidence for predicting the long-term strain of geogrid reinforced soil structures.

PREFACE

Part of this research study has been published in three conferences papers, and form the basis for two journal publications that are in preparation:

1. Fannin R. J., Quinteros S. and Vaslestad J. (2013). Durability of geosynthetic reinforcement: exhumation of a geogrid from a sloped reinforced soil wall after 25 years. Geo-Montreal, Canada, 6 pages.
2. Fannin R.J, Quinteros, Vaslestad J., Ahmed T. (2014). Behaviour of a geosynthetic reinforced soil slope: a 25-year field study. 10th International Conference on Geosynthetics. Berlin, Germany, 9 pages.
3. Fannin R. J. and Quinteros S. (2015). Credible soil strength of reinforced retaining structures. XVI European Conference on Soil Mechanics and Geotechnical Engineering ECSMGE, Edinburg, Scotland, 6 pages.
4. Fannin R. J., Quinteros S. Durability of reinforcement from a sloped wall after 25 years, (in-preparation).
5. Fannin R. J., Quinteros S. and Dyvik R. Performance-based observations: implications for design of reinforced retaining structures, (in-preparation).

My contribution to each publication, and the location of that content within this thesis is given below:

- For the three conference papers I delivered key information, including: literature review, description of the study, and preliminary results. I also conducted inspection of the exhumed geogrid, and performed some laboratory index tests.

- For the two journals articles in-preparation, I performed advanced shear strength tests at the University of British Columbia (UBC) and at the Norwegian Geotechnical Institute (NGI) in Oslo, including all data reduction and much of the analysis. I also performed a back-analysis of the reinforced slope and compared those results against the findings of the laboratory tests.

For all publications (except the second), I wrote most of the preliminary manuscripts in collaboration with my research supervisor, Dr. R. J. Fannin and, where appropriate, received additional input from the other co-authors.

TABLE OF CONTENTS

LIST OF TABLES

LIST OF FIGURES

LIST OF SYMBOLS

Symbol	Name	Unit
B-value	Skempton pore water pressure parameter	-
b	relative position of intermediate principal stresses	-
C_u	coefficient of uniformity	-
C-value	specific extension modulus of membrane	-
CO_2	carbon dioxide	-
D	moment arm of T_{cal} about the center of rotation	m
Dr	relative density	%
d_{10}	diameter of the soil particles for which 10% of the particles are finer	mm
d_{50}	mean grain diameter	mm
d_{60}	diameter of the soil particles for which 60% of the particles are finer	mm
FS_R	target minimum factor of safety of reinforced slope	-
FS_U	unreinforced slope factor of safety	-
Gs	specific gravity	-
H	height of slope	m
H_{ds}	specimen thickness in direct shear test	mm
H_g	geogrid vertical spacing	m
K_{LS}	earth force coefficient for lineal slip analysis	-
K_{BS}	earth force coefficient for bilineal slip analysis	-
M_D	driving moment about the center of failure surface	kNm
L	specimen length	mm
L_{ds}	specimen length in direct shear test	mm
L_g	geogrid length	m
R	roundness	-
S	sphericity	-
T_{max}	maximum measured force within each geogrid layer	kN/m
T_{mob}	mobilized tensile force	kN/m
T_{cal}	tensile force per unit width	kN/m
U_1	under compaction factor, after Ladd (1978)	-
V_0	initial volume	cm^3
z’	depth were geogrid strain measurements were performed	m
ΔV	volume change	-
$-\Delta\varepsilon_v/\Delta\varepsilon_1$	dilatancy rate	-

γ	unit weight	kN/m^3
$\gamma_{d,max}$	maximum dry unit weight	kN/m^3
$\gamma_{d,min}$	minimum dry unit weight	kN/m^3
γ_{ds}	shear strain in direct shear tests	%
γ_{mob}	mobilized geogrid strain	%
γ_{tx}	shear strain in triaxial tests	%
γ_{ps}	shear strain in plane-strain tests	%
$\delta_{v,ds}$	vertical displacement in direct shear tests	mm
$\delta_{h,ds}$	horizontal displacement in direct shear tests	mm
$\dot{\delta}$	rate of displacement	mm/min
ε_{max}	maximum measured strain within the reinforced steep slope	%
ε_v	volumetric strain	%
$\varepsilon_{v,tx}$	triaxial volumetric strain	%
$\varepsilon_{v,ps}$	plane-strain volumetric strain	%
ε_1	major principal strain	%
$\varepsilon_{1,tx}$	triaxial major principal strain	%
$\varepsilon_{1,ps}$	plane-strain major principal strain	%
ε_2	intermediate principal strain	%
ε_3	minor strain	%
θ	slope batter angle	°
μ	coefficient of friction or adhesion	-
ρ	particle regularity	-
σ'_{oct}	octahedral stress	kPa
σ'_n	normal effective stress in direct shear box	kPa
σ'_1	major principal effective stress in triaxial and plane-strain	kPa
σ'_2	intermediate principal effective stress in triaxial and plane-strain	kPa
σ'_3	minor principal effective stress in triaxial and plane-strain	kPa
σ'_1/σ'_3	principal stress ratio	-
τ	shear stress in direct shear tests	kPa
τ_{max}	maximum shear stress at failure in direct shear tests	kPa
τ/σ'_n	stress ratio in direct shear tests	-
ϕ	friction angle	°
ϕ_{cv}	constant volume friction angle	°
ϕ_{ds}	direct shear friction angle	°
ϕ_{mob}	mobilized friction angle	°

ϕ_p	peak friction angle	°
ϕ_{ps}	plane-strain friction angle	°
$\phi_{p,ds}$	peak direct shear friction angle	°
$\phi_{p,ps}$	peak plane-strain friction angle	°
$\phi_{p,tx}$	peak triaxial friction angle	°
ϕ_{tx}	triaxial friction angle	°
ψ	dilation angle	°
ψ_{ds}	dilation angle direct shear	°
ψ_{max}	maximum dilation angle	°
ψ_{ps}	dilation angle plane-strain	°
ψ_{tx}	dilation angle triaxial	°

LIST OF ABBREVIATIONS

AASHTO	American Association of State Highway and Transportation Officials
ASTM	American Society for Testing and Materials
BS	British Standard
GDS	Geotechnical Digital Systems
HDPE	High Density Polyethylene
ISO	International Organization for Standardization
NGI	Norwegian Geotechnical Institute
LVDT	Linear Variable Differential Transformer
OM	Optical Microscope
OIT	Oxidation Induction Time
PET	Polyester
PP	Polypropylene
SEM	Scanning Electron Microscope
SRL	Schmertmann Research Laboratory
SW	Self-Weight of reinforced steep slope
UBC	University of British Columbia
US-FHWA	United States Federal Highway Administration

ACKNOWLEDGEMENTS

Hereby I would like to acknowledge the invaluable guidance and advice of my research supervisor and friend Dr. Jonathan Fannin. With his capacity for simplifying complex processes and disseminating knowledge, he has permanently influenced both my way of thinking and my approach to problem solving. Throughout this research he has always maintained a clear focus and encouraged my critical review of all results and companion analyses. Addition recognition is given to Rune Dyvik, expert advisor and discipline leader of the Norwegian Geotechnical Institute (NGI) laboratory, for his guidance and supervision while performing advanced soil tests at the Schmertmann Research Laboratory (SRL) at NGI in Oslo Norway. I sincerely appreciate his commitment and supportive attitude. His systematic and precise working style confirmed my appreciation for the role of advanced laboratory testing in geotechnical practice.

I also acknowledge the engagement of Dr. Taiebat, as second reviewer, for improving the interpretation of the research findings. Similarly, I am also very grateful to the faculty members and my graduate student colleagues at UBC for their encouragement and help during the last two years. The Norwegian Public Roads Administration managed the program of fieldwork to exhume the geogrid and sand samples. The contribution of Jan Vaslestad and Tor Helge Johansen to this fieldwork is much appreciated. Moreover, the contribution of Willie Liew and Lynn Cassidy to the laboratory testing on geogrid durability at the Tensar International laboratories in the USA is much appreciated. The financial support of NGI for the internship in Oslo and also the Natural Sciences and Engineering Research Council (NSERC) of Canada support, is acknowledged. Lastly, the aid of the Faculty of Applied Science Graduate Award of UBC, and the Ecuadorian Government through its sponsorship program, is recognized with gratitude.

DEDICATION

To my parents: Yolita Araujo and Raul Quinteros, who instilled in their children the importance of education. They showed us, through their example, the role of courage, perseverance and determination to overcome any challenge in life.

1. INTRODUCTION

1.1 Background

Uncertainty about the appropriate soil strength to be used in design of reinforced soil retaining structures has been a topic of discussion since the emergence of design guidance on the use of geosynthetics as reinforcement, more than three decades ago. Current codes of practice advocate the use of peak strength values obtained from laboratory tests, in direct shear, triaxial or (if appropriate) in plane-strain loading. Moreover, design of reinforced retaining structures is largely based on previous experience and experimental field data from just few (ca. 20) well-documented case studies around the world. Load and strain measurements in those structures are reported to be smaller than expected, which suggests uncertainty in design. Amongst all of those documented structures, only one reinforced steep slope has independent measurements of force and strain: the structure was constructed in Norway in 1987 and its post-construction performance was reported by Fannin & Hermann (1990). In order to improve the current understanding of design practice, this research study presents a series of advanced shear strength tests, in direct shear, triaxial and plane-strain conditions, on the backfill sand of the Norwegian structure, with the purpose of informing a back-analysis of the field performance data. Through the back-analysis, the mobilized strength in the field was back-calculated and compared with the strength of the backfill sand obtained in laboratory testing. Discussion of the findings addresses the implications for design practice. Additionally, durability assessment of geogrid samples that were exhumed as part of this research, some 25 years after completion of construction, is

presented herein, with a companion implication for design practice about the use of isochronous load-strain-time data for predicting the long-term strain of geogrid reinforced soil structures.

1.2 Scope and objectives

This research study addresses the Norwegian reinforced steep slope, the laboratory testing of its backfill soil, and its back-analysis. Additional consideration is given to the durability of the geogrid reinforcement. The main objectives of each part of this study are presented below:

1.2.1 Geogrid durability

- Assessment of durability of exhumed geogrid samples by visual inspection and a series of index and strength tests. Identification of possible physical damage and/or degradation.
- Identification of implications of this durability assessment for current design practice about the use of isochronous load curves for characterizing the long-term strains of uniaxial geogrid reinforcement.

1.2.2 Soil strength

- Perform advanced shear strength tests (in direct shear, triaxial and plane-strain conditions) at stress levels appropriate to the geometry of the steep slope.
- Assess the credibility of the laboratory test data and resulting friction angle by comparing the results with typical empirical correlations and test data reported in the literature.

1.2.3 Back-analysis

Back-analysis is limited to the internal stability of the structure. Two postulated failure modes were considered: a lineal slip and a bilineal slip. The main objectives of the back-analysis are:

- Determine the mobilized strength within the structure an appropriate geotechnical model.
- Test the hypothesis that plane-strain conditions prevail within the Norwegian reinforced steep slope.
- Check if the recommendations of BS-8006, USFHWA and AASHTO on the use of a peak strength value for design are consistent with performance monitoring data of the Norwegian reinforced steep slope.

1.3 Structure of the thesis

The main content of each chapter is as follows:

- Chapter 2 presents a description of the Norwegian reinforced steep slope, making reference to its design, construction and instrumentation. Additionally, the description includes sampling of geogrid and backfill soil conducted in February 2013, in support of this research, and a short comment on reinforcement durability.
- A detailed assessment of reinforcement durability based on testing samples of geogrid reinforcement obtained in February 2013, some 25 years after completion of construction, is reported in Chapter 3.
- The characterization and advanced shear strength tests of samples of the backfill soil are reported in Chapter 4. Analysis and discussion address the significance of experimental results.

- A back-analysis of mobilized strength in the reinforced steep slope is reported in Chapter 5, together with a comparison of this mobilized strength with that obtained from the laboratory testing described in Chapter 4.
- The main conclusions of the investigation, together with its implications for current design practice, are found in Chapter 6.

2. NORWEGIAN REINFORCED SOIL SLOPE

A detailed report on the design, construction and instrumentation of the sloped reinforced soil wall is given by Fannin (1988), together with a summary of performance monitoring data for the initial period after completion of construction (Fannin & Hermann, 1990), and over a longer period of time (Fannin, 1994; Fannin, 2001). In order to provide significant background information to the current research study, a short description of this earlier work is given herein.

2.1 Description

The structure is located near to the town of Skedsmo, around 25 km northeast of Oslo, Norway (N60° 0.950', E11° 3.345'). The steep (2V:1H) sloped reinforced soil wall is 20 m long and 4.8 m high, and was constructed into the toe of an existing hill-slope (see Figure 2.1). It comprises two sections, termed Sections J and N, each of which is 10 m long and with a different arrangement and spacing of geogrid reinforcement. The current research study considers only Section 'N' of the structure (see Figure 2.2). Construction of the sloped wall was completed in July 1987. Following 28 days of self-weight loading, a load-unload cycle of surcharge loading was applied over 63 days using water tanks that were filled in stages on the crest of the sloped-wall. Thereafter, a permanent surcharge was applied by means of a 3 m high berm, which was built on top of the structure in October 1987 (Fannin & Hermann, 1990). For simplicity, the present study is limited to a consideration of the self-weight (SW) loading condition only of Section N of the structure.

2.1.1 Backfill soil and slope construction

A uniformly graded clean sand with trace of fine gravel, called Skedsmo sand, was used as backfill in the reinforced steep slope. The measured characteristics of this sand (Fannin, 1988) were: bulk unit weight (γ = 17 kN/m^3), maximum and minimum dry unit weight after the NGI procedure ($\gamma_{d,max}$ = 17.76 and $\gamma_{d,min}$ = 14.16 kN/m^3, respectively), median grain size (d_{50} = 0.2 mm) and coefficient of uniformity ($C_u = d_{60}/d_{10}$ = 2.6). During construction of the slope in 1987, the sand was placed with a front-end loader (Volvo type BM 4500) that was not permitted to drive on the zone of soil reinforcement. The sand was spread with a mini-excavator (Takeuchi type TB36) that was permitted to operate in the zone of soil reinforcement where the geogrid was covered by a minimum thickness of 350 mm of loose sand. The sand was wetted using the hose-supply from a water-truck, and then densified by compaction using a vibrating plate (Dynapac type LG450) to a dry density greater than 92 % of the maximum value from the Standard Proctor test (ASTM D698) at a water content between 5 and 10 %. Nuclear densometer measurements performed during construction of the slope establish that a relative density (D_r) of approximately 50 % was achieved in construction.

2.1.2 Reinforcement

A uniaxial geogrid, Tensar SR 55, was used in construction of Section 'N'. In total, 8 layers of reinforcement (termed layers N1 to N8) were placed at a uniform vertical spacing of 0.6 m. Each layer of geogrid reinforcement is 2.2 m long, yielding a length/height ratio of L_g/H_g = 0.46. A detailed description of the geogrid characteristics, together with an assessment of its durability is given in Chapter 3.

2.1.3 Instrumentation and performance (1987 - 1988)

The structure was instrumented to monitor its post-construction performance. Vibrating-wire load cells were used to measure the force per unit width in the reinforcement, while Bison inductance coils were used to measure the strain in the reinforcement and adjacent backfill sand. Temperature of the backfill sand was monitored using thermistors. The instrumentation scheme was configured to yield independent measurements of force and strain over time and at known temperature (see Figure 2.2 (b), (c) and (d)). This permitted a comparison of field performance data with laboratory isochronous load-strain data from creep testing of the geogrid. Instrumentation details are found in Fannin (1988).

During the field monitoring of self-weight loading conditions, small geogrid strains were reported. The measured tensile strains in each layer of reinforcement ranged between 0.3 and 0.7 %, and were typically about 0.5 %. The companion measured tensile forces in each layer of reinforcement ranged between 1.0 and 2.3 kN/m, and were typically about 2 kN/m: the sum of the mobilized forces T_{mob} = 15.3 kN/m (see Table 2.1). Furthermore, the measured geogrid strain was found comparable in magnitude with the soil strain, inferring a good interlock between reinforcement and backfill. Displacements of the face of the structure were monitored during and immediately after construction and were used to define movement qualitatively. Typically the horizontal displacements have exceeded vertical displacements, with outward movement predominant in the upper parts of the slope (Fannin and Hermann 1990). A very general interpretation of the measured displacements, in combination with the geometry of the structure, would suggest that plane-strain conditions likely prevail within the structure. This study examines the evidence from strength testing of the backfill soil in support of a mobilization of the friction angle in plane-strain.

A representative vertical stress (σ'_1) at the general location in the structure where maximum geogrid strains were measured (see Figure 2.2 (b)), can be estimated from the relation between the soil unit weight (γ) and the overburden depth below the sloped face of the structure (z'):

$$\sigma'_1 = \gamma \cdot z' \cdot \approx 17 \frac{\text{kN}}{\text{m}^3} \cdot 1.5 \text{ m} \approx 25\ kPa \quad (1)$$

For layer N8, $\sigma'_1 \approx$ 10 kPa, for layer N7, $\sigma'_1 \approx$ 20 kPa, and for layers N6 to N1, it varies between $26 < \sigma'_1 < 27$ kPa. A value of $\sigma'_1 \approx$ 25 kPa is therefore believed to be representative of the stress conditions along a candidate locus of slip in the reinforced steep slope.

No codes of practice were available for design when the slope was built in 1987. Accordingly, at that time, the structure was designed against progressive failure using ϕ_{cv} = 33º obtained from direct shear tests (see Fannin, 1988). Thereafter, analysis of the field performance monitoring data (Fannin & Hermann, 1990), suggested a friction angle of ϕ = 35 to 40º was likely mobilized in the backfill soil. Moreover, in agreement with the field observations, the mobilized strength was expected to be a plane-strain friction angle, taking into account the recommendations of Jewell & Wroth (1987):

$$\phi_{ps} = \tan^{-1}(1.2 \tan \phi_{cv}) = \tan^{-1}(1.2 \tan 33) = 38\,° \quad (2)$$

In the absence of any comprehensive testing of the backfill soil at that time, little additional comment was made about the mobilized value of soil strength, nor was any further consideration given to matters of strain and stress compatibility in plane-strain conditions.

2.2 Field sampling in 2013

A program of field sampling was conducted at the Norwegian site, over a period of two days in February 2013, when the daily maximum air temperature was approximately -5 °C. Seasonal

frost penetration had frozen the backfill sand to a depth of approximately 0.75 m. The site was covered in snow that was approximately 0.25 m deep.

2.2.1 Backfill soil sampling

Sampling of the backfill sand was done in Section 'N', and it was facilitated by the site layout providing for easier access to that end-location of the structure. Excavation proceeded in a 'top-down' direction, from the horizontal crest of the 4.8 m high sloped-wall immediately adjacent to the lateral toe of the permanent surcharge berm (see Figure 2.4 (a)). Soil samples were taken at select elevations during the process of top-down excavation. As noted earlier, each layer of geogrid is separated by a vertical spacing of 0.6 m and the grab samples of backfill sand were taken at the mid-height of the compacted soil between each geogrid layer. Accordingly, Sample S7-8 was taken between geogrid layers N8 and N7 (see Figure 2.4 (b)). In total three samples of backfill sand were obtained.

Soil samples were sent to NGI and UBC, for material characterization and advanced soil strength tests. A photomicrograph of Skedsmo sand, which was obtained using an optical microscope (Meiji EMZ-5TR / Moticam-2300) at UBC, is shown in Figure 2.3. The roundness (R = 0.43), sphericity (S = 0.60) and particle regularity (ρ = 0.49) were assessed after the Krumbein & Sloss (1963) definition. The grains are categorized as very angular (after the definition of Tsomokos & Georgiannou, 2010). Using an X-ray powder diffractometer (Siemens D5000 Vantec detector and Bruker D8 Focus: LynxEye detector), the main minerals were identified: quartz ca. 70%, feldspar ca. 20%, mica ca. 5% and others 5%. The specific gravity (G_s = 2.67) was determined after ASTM-D854-10.

2.2.2 Geogrid sampling

Geogrid sampling was also done in Section 'N'. The exhumed geogrid, Tensar SR55, is a high-density polyethylene (HDPE) uniaxial geogrid. The excavator (Komatsu type PC13) peeled off the frozen ground to a depth of 0.75 to 1.0 m, taking with it the uppermost geogrid layer N8. Geogrid layer N7 was 'assigned' as a sacrificial layer to be used for development and refinement of a method for sequential machine- and hand-excavation to expose the subsequent layers of reinforcement, as described herein (see Figure 2.5 (a)).

The backfill sand was carefully removed by machine-excavation, in a series of horizontal cuts. The remaining depth to the underlying layer of geogrid was checked periodically by advancing a narrow slit-shaped trench, by hand-excavation using a spade. The direction of hand-excavation was always orthogonal to the face of the sloped-wall, thereby ensuring the action of the spade remained parallel to the roll length (longitudinal) direction of the geogrid. This limited the possibility of the spade inadvertently catching one of the ribs, an undesirable action that was experienced by trial-and-error on the sacrificial layer N7.

Machine-excavation ceased when the cover thickness of backfill sand was reduced to approximately 15 cm. The remainder of the backfill was then removed by hand-excavation, using a shovel to move the bulk of the sand, and a combination of spade and soft-sweep push-broom to remove all of the remaining sand and expose the top surface of the geogrid layer (see Figure 2.5 (b)). Figure 2.5 (b) was taken when the process of excavation had advanced down to geogrid layer N3, the lowermost layer that was sampled: it shows the 2V:1H sloped face of the wall, the exposed vertical face of the top-down cut, an excavated stockpile of backfill sand in front of the sloped wall, and three adjacent 1 m wide panels of Tensar SR55 geogrid.

At the face of the sloped wall, the ground was frozen to a thickness of approximately 0.75 m. Consequently, it was not possible to exhume the complete 2.2 m length of reinforcement. Instead, the individual ribs of the geogrid were cut, one-by-one, with a hand-held snipper at the location where the geogrid met frozen ground. Typically, a 1.25 m length of geogrid was obtained by this method of exhumation and sampling. In total, 10 panels of geogrid, each 1 m wide and approximately 1.25 m long, were removed from layers N5, N4 and N3. They were labeled on-site, then rolled and placed in an industrial strength cardboard tube for shipment to Tensar International in the USA for materials testing. Additional geogrid samples were taken from layers N6, for detailed visual inspection and description at UBC. The exhumed geogrid area was 13.7 m^2, which is around 8 % of the total surface area of the installed geogrid in section N.

Table 2.1 Measured values of strain and force in the geogrid during self-weight loading (Fannin & Hermann 1990)

	Measured geogrid strain	Measured tensile force
Geogrid layer	ε_{max} (%)	T_{max} (kN/m)
8	0.66	2.26*
7	0.56	1.92
6	0.37	1.46
5	0.52	2.00
4	0.63	2.34
3	0.43	2.01
2	0.43	2.25
1	0.30	1.06
Average	0.48	1.9
$T_{mob} = \sum T_{max}$ (kN/m)		15.3

* Deduced from a consideration of layer 7

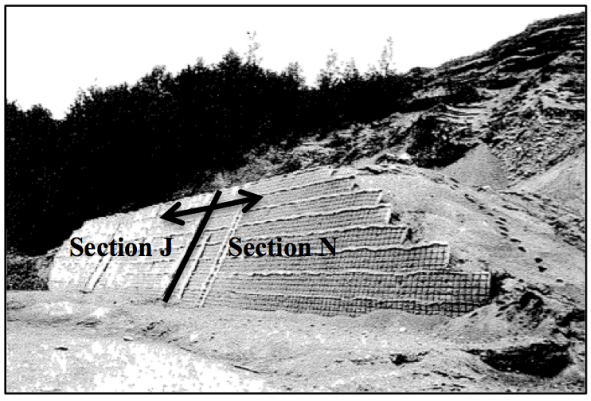

Figure 2.1 Reinforced steep slope after construction in 1987 (Fannin & Hermann 1990)

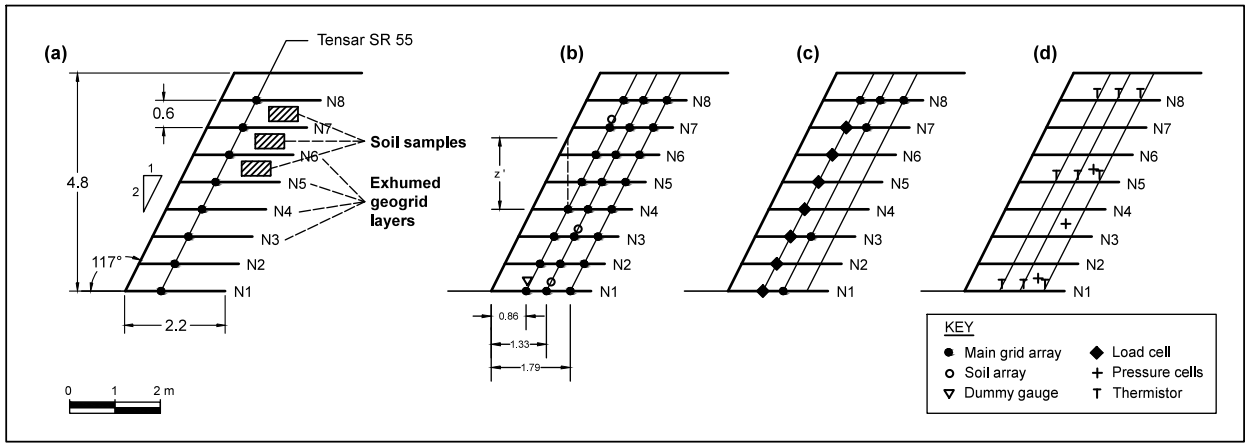

Figure 2.2 Section N: (a) arrangement of geogrid reinforcement and materials sampling, (b) strain monitoring, (c) force monitoring, and (d) temperature monitoring

Figure 2.3 Photomicrograph of Skedsmo sand

Figure 2.4 (a) Excavation into Section 'N', (b) location of the soil samples

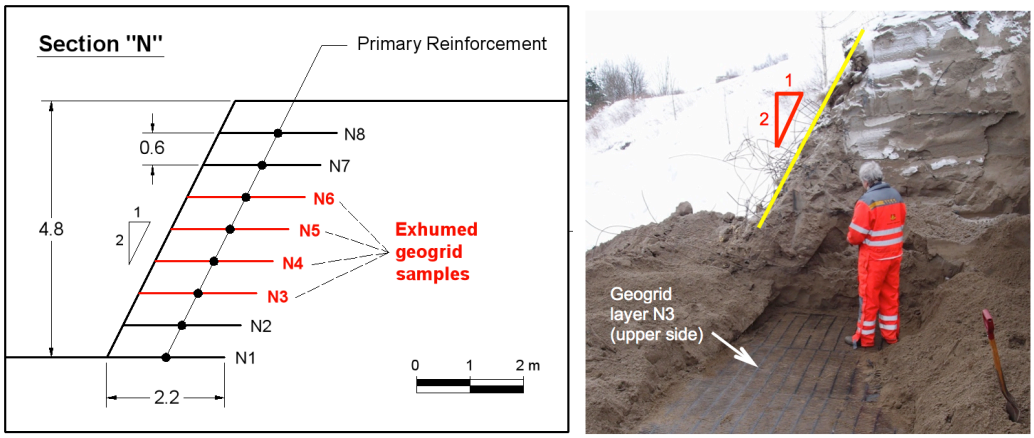

Figure 2.5 Field sampling: (a) sketch of exhumed geogrid layers; (b) exhumation of layer N3

3. DURABILITY OF THE TENSAR SR 55 GEOGRID REINFORCEMENT AFTER A 25 YEARS BURIAL PERIOD

3.1 Introduction

In the selection of a long-term value of strength in design practice, reduction factors that differentiate between installation and durability are typically considered. Such factors seek to address the possible decrease of reinforcement strength, and are specified in national guidelines and codes of practice (see US-FHWA, AASHTO and BS-8006). However, the limited number of long-term studies on reinforcement durability have encountered challenges in trying to distinguish between causes of strength loss. Harney and Holtz (2006) reported on the difficulty of distinguishing between strength loss due to installation damage at the time of construction and degradation over the service life of a woven polyester geotextile used as reinforcement in a Swedish bridge-embankment, and exhumed after 30 years, because no geotextile samples were retrieved immediately after installation. They reported evidence of severe damage, from visual inspection, and identified a significant reduction in the peak strength modulus (around 50%) and elongation strain at failure from experimental data of wide-width tensile tests on exhumed samples compared with results on stored samples of the virgin geotextile. Bright et al. (1994) and Wayne et al. (1997) reported on the properties of high-density polyethylene (HDPE) geogrid exhumed from a concrete-faced reinforced soil retaining wall in Arizona, USA after 8 and 11 years in-service respectively. The geogrid was installed in an elevated temperature environment that could have possibly accelerated degradation. The basis of evaluation was to compare material properties, obtained from visual inspection, geometry characterization, material

composition and tensile strength (including ultimate tensile strength/strain and creep response to 1,000 hours), with values from archived samples. Again, and somewhat unfortunately, no distinction could be made between installation and durability in this study. However, no significant changes in either the physical or material properties of the geogrid, or morphological properties of the HDPE, were found. Onodera et al. (2004) reported on the durability of various reinforcements (including glass fiber, and HDPE) that were exhumed after 7 and 12 years in-service from four different types of retaining walls in Japan. Visual inspection confirmed the good condition of the exhumed samples. Neither a quantitative geometry evaluation, nor creep load tests were reported. However, tensile strength capacity was investigated by rapid tensile load tests. Additionally, material composition was assessed from chemical degradation tests by submerging the geogrid samples in different fluids before tensile tests were performed. In this study, the differentiation between installation and durability was not mentioned and therefore it is assumed that installation damage was not assessed. However, even though the scatter in maximum tensile strength was found significant, an overall high strength retention rate indicated no degradation of the geogrids. Jenner & Nimmesgern (2006) reported findings on the durability of HDPE geogrid reinforcement from a railway embankment in Germany after 10 years. The geogrid was subjected to extreme conditions of static and dynamic loading. From visual observation, severe damage of the ribs was reported in the form of surficial cracks and fissures of the near-surface layers directly under the railway tracks. No geometry assessment was reported. However, comparison of quality control tests results between the exhumed samples and virgin geogrid samples indicated a relatively small decrease in tensile strength. From the linear relationship between tensile strength and strain of the quality control tests, it was assumed that no changes had occurred in material composition over the years. Since installation damage was

not assessed after construction of the embankment, the decrease of strength was attributed to installation damage, as well as static and dynamic loading. Taken collectively, the individual studies are in general agreement with the more extensive study of Elias et al. (2000) on durability of geogrids and other high strength geotextiles used as reinforcement. Those materials were exhumed as long as 20 years after being installed at 12 different sites (24 geosynthetic samples in total including HDPE, PP and PET). Elias et al. suggested, based on visual observation, index tests and tensile strength tests, that strength loss can be mainly attributed to installation damage.

Given the limited body of data published on geogrid specimens exhumed after more than 20 years in-service, and the fact that a differentiation between installation and durability has not always been possible (see Table 3.1), and given desire for greater confidence in understanding the long-term behaviour of geosynthetic reinforcement, the current research study presents a durability assessment of the geogrid exhumed from the Norwegian reinforced sloped soil wall, after about 25 years of serviceability. The main objectives of this investigation are: to i) identify installation damage based on visual observation, ii) quantify material properties in terms of geometry, composition and tensile strength, iii) report on any changes of geogrid properties over time, and iv) based on the findings, comment upon the implications for design practice. Installation damage of the exhumed samples was assessed at the University of British Columbia (UBC) in Vancouver, Canada, while material composition was evaluated at an independent laboratory (Sageos/CTT in Quebec, Canada) and tensile strength was assessed at the Tensar International laboratories (geogrid manufacturer) in Atlanta Georgia, USA with a third-party inspection.

3.2 Testing and characterization of the geogrid samples after 25 years

Typical dimensions of the geogrid, and a sketch of its geometry, are found in Table 3.2 and Figure 3.1 respectively. The durability assessment of the obtained geogrid samples included: a visual inspection, material composition, and tensile strength tests. Results of the durability assessment are presented below.

3.2.1 Visual inspection

All exhumed geogrid specimens were visually examined in-situ. However, specimen N6 was not only carefully visually inspected but also examined in detail using a scanning-electro-microscope (SEM: Philips XL30 with Bruker Quanta 200 energy-dispersion X-ray microanalysis system with Xflash 4010 SDD) at UBC.

From the visual inspection, a high frequency of low magnitude abrasions were identified (scratches of variable lengths, typically less than 0.1 mm deep), see Figure 3.2. Moreover, a very low frequency of medium magnitude abrasions were also encountered (pits, and gouges that were typically 0.2 to 0.5 mm deep and 2 to 15 mm long), see Figure 3.3.

It was not possible to distinguish if the installation or the exhumation process produced the abrasions. However, due to the minor nature of these features of the geogrid, in form of surficial abrasions, it is concluded that no significant installation damage had taken place at the time of construction.

3.2.2 Material composition

In order to determine any changes on geogrid geometry, measurements of aperture size, rib

thickness, cross machine direction (CMD) bar thickness, rib width and CMD bar width were compared against typical values of the geometric attributes reported by the manufacturer. Measurements were performed on four specimens of layer N3 and three specimens each of layers N4 and N5 at the Tensar International laboratories in Atlanta, USA. The measurements varied within 0.1 and 4 % of the typical values (see Table 3.2). This evidence suggests that there is no significant change of the geogrid geometry.

Carbon black content of specimens N3, N4 and N5 was determined in accordance with ASTM D4218 at the Tensar International laboratories. Those deduced values exceeded the typical values reported by the manufacturer by almost 40 % (see Table 3.2). In addition, UV-resistance was determined in accordance with ASTM D4355-07 on five specimens of layer N4 by the independent testing laboratory 'Sageos/CTT' in Quebec, Canada. The maximum rib tensile strength increased in 2% after UV-exposure, while the elongation at maximum strength increased by 11 % (see Table 3.2). Although historical UV data are not available for purposes of comparison, the tests on exhumed N4 specimens show a high resistance to UV after the elapsed time of 25 years.

Index testing to ASTM D4972-01 indicates the backfill sand has a pH = 8.3, which is believed unlikely to have had any adverse chemical influence of the durability of the geogrid. Additionally, scanning electron micrographs of Skedsmo sand are shown in Figure 3.4. Moreover, the soil temperature was found on average to be 8 ºC during 10 years of monitoring after construction of the reinforced structure: the maximum average temperature was 14 and the minimum average 2 ºC, see Fannin (2001).

The deduced high carbon black content, the inferred good UV-resistance, the pH of the backfill

and the temperature regime in service imply no significant potential for physical degradation of the polymer.

3.2.3 Tensile strength

Rapid loading creep (RLC) tests to ISO 13431:1999 were performed on specimens N3 and N5 in the Tensar International laboratories, with a third-party inspection of the testing. Different magnitudes of tensile load (TL) were applied to the test specimens (TL = 8.8, 15.4,17.8,19.8, and 24.2 kN/m for layer N3, TL = 8.8, 17.8 and 24.2 kN/m for layer N5), and the registered elapsed times were t = 1, 10, 100, 1,000, and 10,000 hours. The RLC tests provided load-strain-time data at a constant temperature of T = 20 ± 2°C, and are presented in the form of isochronous curves. Tests results from the current study are compared with typical test data reported by the manufacturer for the Tensar SR55 geogrid in 1987 (see Figure 3.5). There is good agreement in the load-strain response between exhumed specimens N3 and N5: for example, at the largest value of load per unit width of 24.2 kN/m, the difference between the total strain in the N3 and N5 test specimens is 0. % strain at t = 1 hour, 0. % strain at t = 10 hours, 0. % strain at 100 hours, 0. % strain at 1,000 hours, and 0. % strain at 10,000 hours. Accordingly, the difference between then is less than or equal to 7.6 % of the total strain value. Moreover, there is a reasonable agreement between the N3 and N5 test specimens and the typical test data from manufacturer (see Figure 3.6). A best-fit line through the total strain of the N3 and N5 test specimens is described by the following relation: $\varepsilon_{exh} = 0.92 \cdot \varepsilon_{typ}$. Accordingly, the total strain in test specimens of the exhumed geogrid layers, for all values of tensile load and elapsed time to 10,000 hours, are consistently less than the typical values of total strain values by 10 % on average. Moreover, strain increments were calculated from the total strain on the exhumed

specimens, and also from the typical values, for increments of 1-10, 1-100, 1-1,000 and 1-10,000 hours (as shown schematically in Figure 3.7). Strain increments on specimens from the exhumed layers, at 1-10 hours, are in reasonably good agreement with the typical values reported by the manufacturer. Yet more encouragingly, strain increments at 1-100, 1-1,000, and 1-10,000 hours are in excellent agreement with typical values (see Figure 3.8), and all of the data are described by the following relation: $\Delta\varepsilon_{exh} = 1.03\Delta\varepsilon_{typ}$. Taken collectively the evidence in Figure 3.6 and Figure 3.8 suggest the isochronous load-strain response in the exhumed specimens compares very well with the typical behaviour reported by the manufacturer.

3.3 Implications for design

The British Standard (BS-8006) gives explicit consideration to a serviceability limit state, which is expressed as a limit value on the magnitude of permissible post-construction strain over the service life of a structure. Isochronous load-strain curves are used for purposes of estimating the post-construction strain in a reinforced soil retaining structure. The difference between 'the end of construction total strain' and 'the design life total strain' is defined as the strain increment. The observed excellent agreement between strain increments in this study validates the use of isochronous load strain curves for estimating long-term strains, as suggested by BS-8006.

3.4 Conclusions

From the presented evidence on geogrid durability, after the elapsed time of 25 years, the following conclusions are drawn.

- Visual inspection suggests no major physical damage during installation. Therefore, it

would appear reasonable to attribute any changes in strength of the geogrid to the elapsed time of 25 years.

- Index testing to establish geogrid geometry, carbon black content, UV-resistance, pH of backfill and temperature suggest no significant physical degradation
- Rapid loading creep tests data show excellent agreement between exhumed and typical values, implying no significant durability degradation in the geogrid of the Skedsmo structure. Accordingly, isochronous load-strain-time data can be used with confidence for predicting the long-term strain of geogrid reinforced soil structures.

Table 3.1 Case histories of durability assessment of geosynthetics used as reinforcement

Case History	Structure	Reinforcement	Elapsed time (yrs.)	Forensic evidence					Commentaries
				Visual inspection	Geometry	Composition	Tensile strength	Creep response	
Bright et al. (1994) and Wayne et al. (1997)	Retaining wall	Geogrid (HDPE)	8 and 11	X	X	X	X	X[1]	No differentiation between installation damage and durability. However, no significant changes on geogrid properties were reported
Elias et al. (2001)	Retaining walls, embankments and roads	24 samples (HDPE, PP and PET)	up to 25	X	X	X	X	n/a	Differentiation between installation damage and durability on some but not all samples. No creep tests reported
Onodera et al. (2004)	Retaining walls	Geogrids (various)	7 and 12	X	X	X	X	n/a	No differentiation between installation damage and durability. No creep tests reported.
Jenner and Nimmesgern (2006)	Embankment	Geogrid (HDPE)	10	X	X	X	X	n/a	No differentiation between installation damage and durability. No creep tests reported.
Harney and Holz (2006)	Embankment	Geotextile (PP)	30	X	X	X	X	n/a	Installation and degradation could not be separated. Significant reduction of tensile modulus reported.
Current study	Sloped wall	Geogrid (HDPE)	25	X	X	X	X	X[2]	Indirect differentiation between installation damage and durability. However, no significant changes on geogrid properties were found.

[1] 1,000 hrs. creep tests
[2] 10,000 hrs. creep tests

Table 3.2 Material properties of original and exhumed geogrid

Parameter	Method	Unit	Original material[1]	Exhumed layer[2]		
				N3	N4	N5
Material geometry						
Aperture size	Calipered	mm	140	140.5	140.9	139.8
Rib thickness			0.95	0.99	0.97	0.99
CMD bar thickness			2.5 – 2.7	2.7	2.7	2.7
Rib width			6.7	6.5	6.5	6.5
CMD bar width			16	16.1	16.1	16.1
Composition						
Carbon black content	ASTM 4218	%	2	2.6	2.7	2.7
UV-Resistance[3]						
Initial maximum rib tensile strength	ASTM D4355	N	n/a	n/a	1267.5	n/a
Elongation at maximum strength		**%**			13.7	
Maximum rib tensile strength after 500 hrs		N			1293.8	
Elongation at maximum strength after 500 hrs		**%**			15.3	

[1] Typical values reported by the manufacturer

[2] Average results from 3 or more samples of each layer

[3] Exposition cycle: 90 min of light only, followed by 30 min of water spray and light, Temperature T = 65±2ºC, Relative Humidity RH = 50±5% and irradiation 0.35 W/m2/nm @ 340 nm

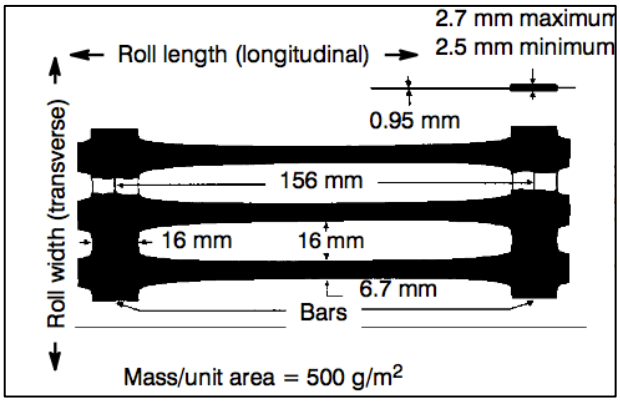

Figure 3.1 Geogrid Tensar SR55 (from manufacturer literature)

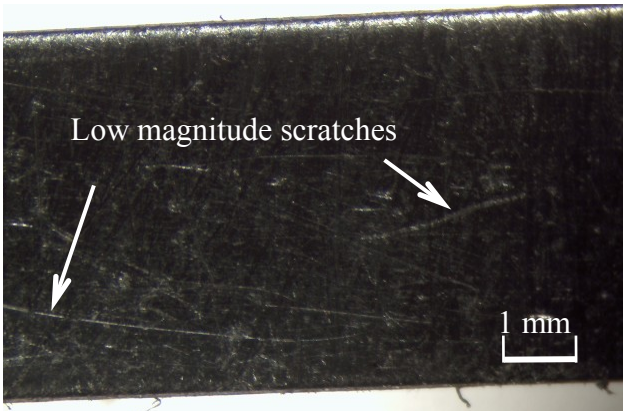

Figure 3.2 Low magnitude surficial abrasion on upper side of geogrid layer N6

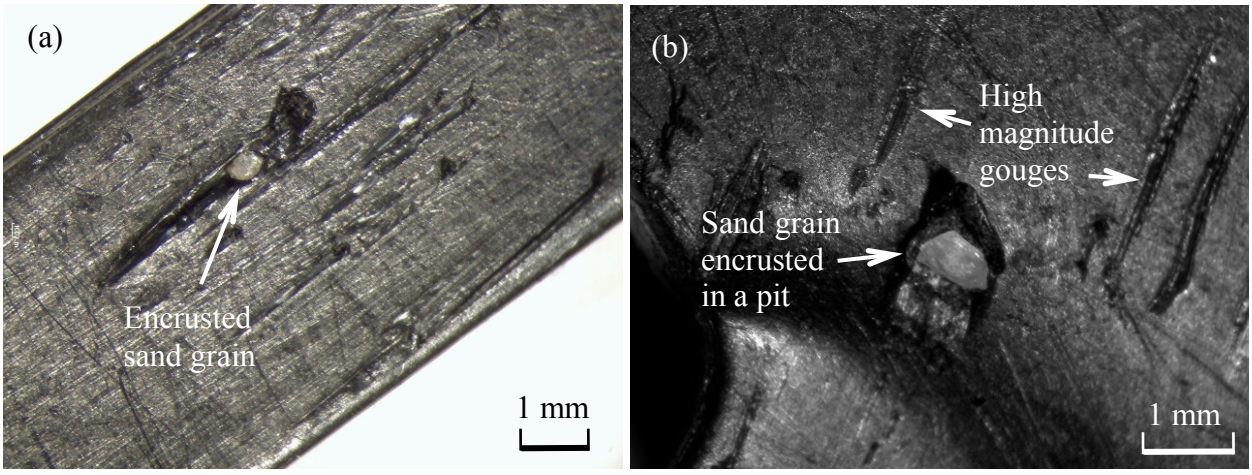

Figure 3.3 High magnitude surficial abrasion on upper side of geogrid layer N6 in (a) the longitudinal rib and (b) the transverse bar of the geogrid

(a) (b)

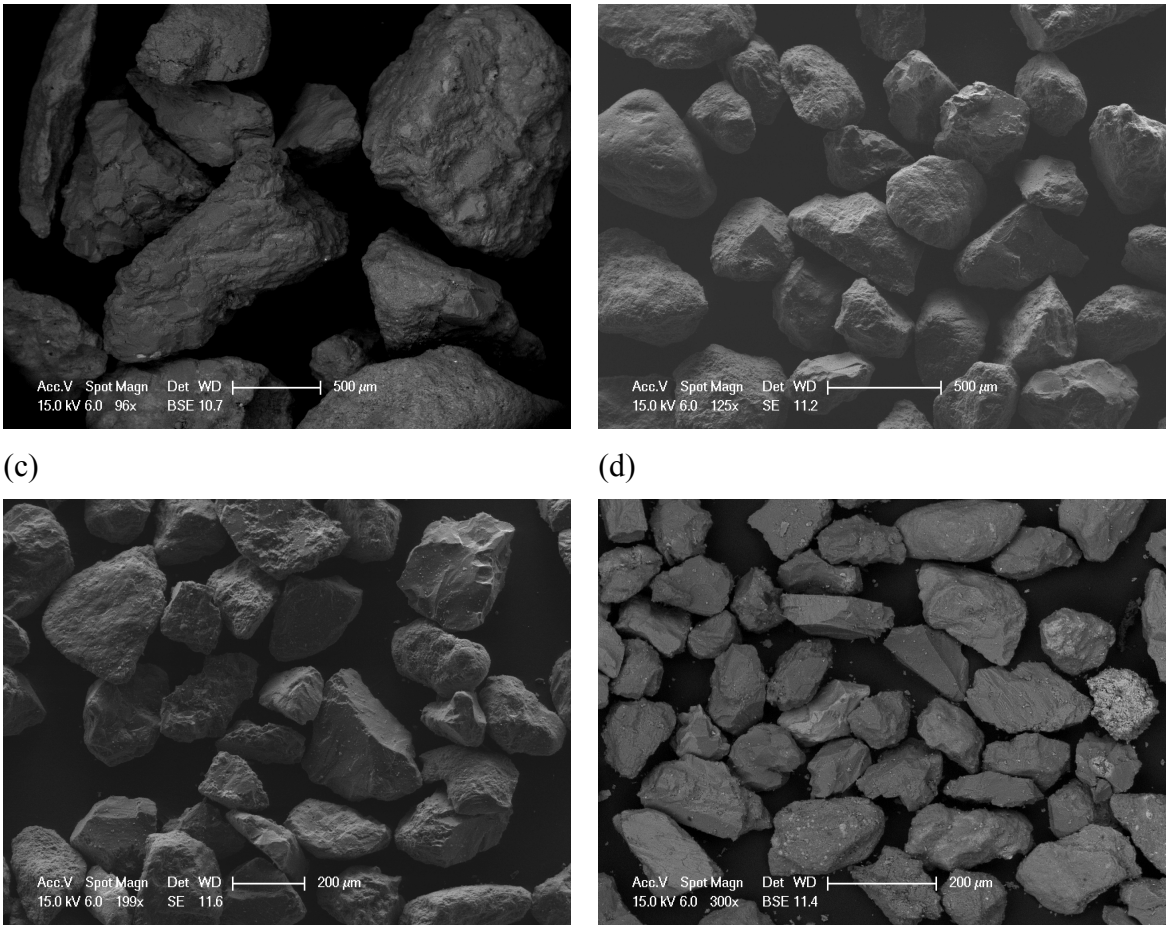

(c) (d)

Figure 3.4 Scanning electron micrographs of Skedsmo sand for different grain sizes: (a) d > 500 µm; (b) 250 < d < 500 µm; (c) > 125 < d < 250 µm; (d) 125 < d < 75 µm

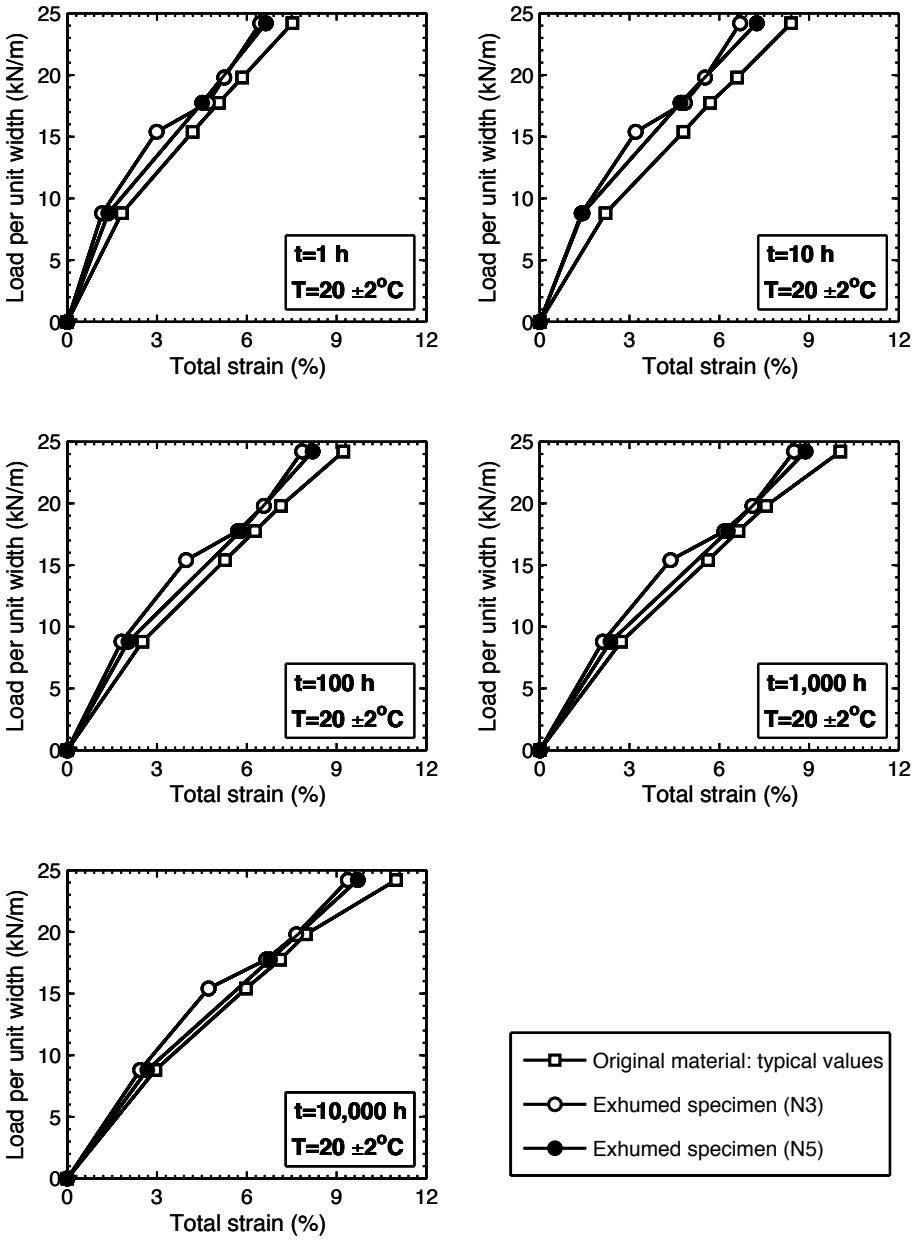

Figure 3.5 Isochronous load-strain curves, original material vs. exhumed samples (measured values from specimens N3 and N5)

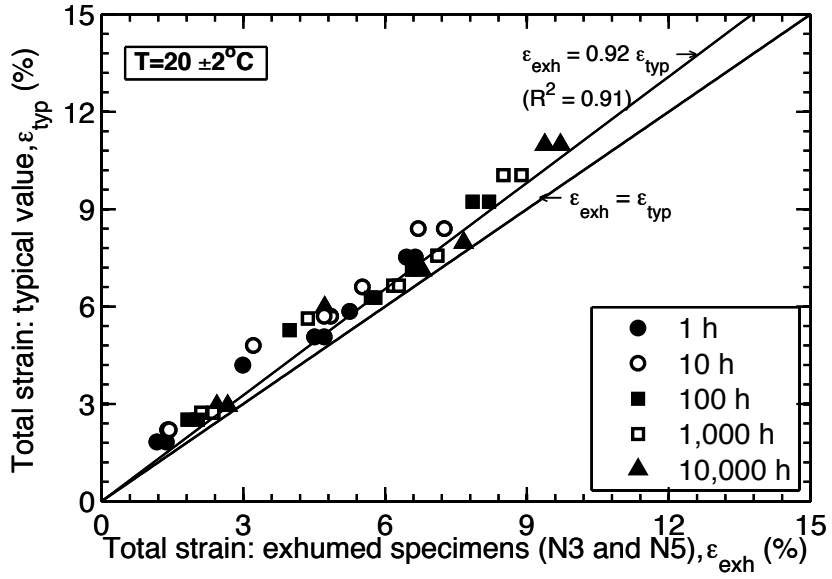

Figure 3.6 Total strains comparison between original material and exhumed geogrid specimens N3 and N5

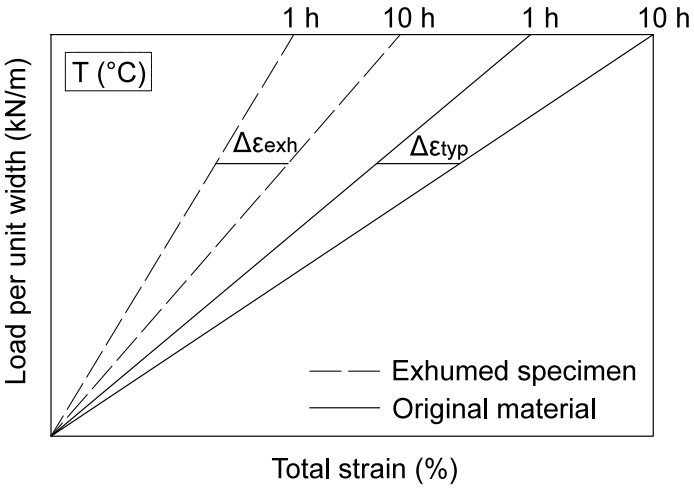

Figure 3.7 Schematically illustration of the calculation of strain increments for 1-10 hours

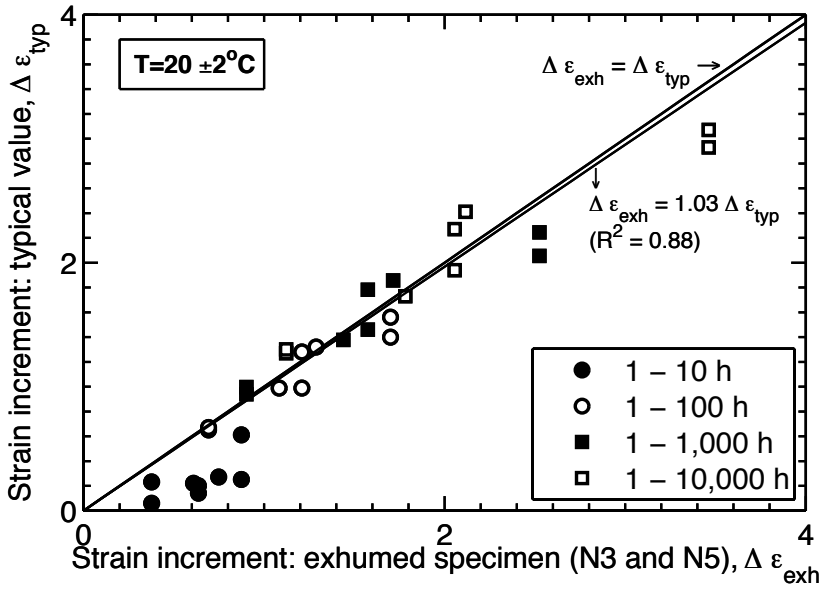

Figure 3.8 Comparison between strains increments of original material and exhumed geogrid specimens N3 and N5

4. SOIL STRENGTH

4.1 Introduction

Drained direct shear, triaxial and plane-train tests were performed on the samples of Skedsmo sand. Prior to testing, the samples were combined by mixing and any particles larger than 4 mm (less than 2 % of the total sample mass) were removed, in accordance with the recommendations of Head (1982) that the maximum particle should not exceed 3.35 mm because of dimensional-compliance of the test specimen in each device. The direct shear tests were done at UBC, whereas the consolidated drained triaxial compression and plane-strain tests were carried in the SRL at NGI. Since drained conditions are prevalent in the backfill and also in the testing, all values of stress and shear strength are reported herein with reference to effective values. Moreover, the sign convention is: compression is considered positive (+), while dilation is considered negative (-). A series of tests was performed in each tests device at almost the same value of effective stress ($\sigma'_n = \sigma'_3$ = 4, 10, 25, 50, 100, 200 and 300 kPa), where σ'_n is the normal stress in direct shear tests and σ'_3 is the cell pressure in triaxial and plane-strain tests. Test specimens were reconstituted to a target relative density $Dr \approx 52$ %, which is comparable to that achieved during construction of the reinforced steep slope in the field.

4.2 Direct shear tests

Direct shear tests were performed using a Durham Geo-Enterprises apparatus (SN 4042, model 2001D). Soil specimens were reconstituted in a square box (100 mm length x 100 mm width). A photo of the equipment is shown in Figure 4.1(a), together with a companion schematic drawing

of the test specimen in Figure 4.2(a). A normal stress $\sigma'_n \leq 11$ kPa was applied using dead weight loading. Above this value, an air pressure system was used to apply σ'_n. All tests were performed a constant rate of displacement $\dot{\delta}$ = 0.08 mm/min, with the specimen being sheared by pulling the lower box to a maximum horizontal displacement of $\delta_{h,ds}$= 5 mm. Shear force was measured using a S-type load cell, type CAS Model SBA-1.5klb, while $\delta_{h,ds}$ and the vertical displacement ($\delta_{v,ds}$) were measured using digital displacement transducers type Novotechnik TR 50, to ± 0.01 mm.

4.2.1 Specimen reconstitution and testing procedure

Soil behaviour is directly influenced by its fabric and therefore by the reconstitution technique used to prepare a laboratory specimen (Oda, 1972; Vaid & Saivathayalan, 2000). Ideally, the reconstitution technique should closely reproduce field conditions. In the case of compacted fill structures like the reinforced steep slope, tamping is believed to be an appropriate reconstitution technique. In the direct shear box, specimens were reconstituted by dry tamping and supplementary vibration to a relative density of $51 < Dr < 56$ %. Three layers of equal weight were poured at zero drop height into the shear box. Each layer received fifty blows of the tamping weight. Using the top ribbed plate of the direct shear box, a normal stress of 25 kN/m^2 was applied and finally a hand-held vibration device (an electro motor-driven Wen type 1) was brought into contact with the shear box for 30 seconds. In order to control the initial Dr, the change in specimen thickness was measured using a caliper device.

4.2.2 Corrections and calculations

The values of shear stress (τ) were corrected taking into account the continuously changing

planar area of the specimen during a test. The values of σ'_n were corrected for the second order mechanical friction following the recommendation of Lehane & Liu (2013) to include the weight of the upper-half of the shear box. Shear strain (γ_{ds}) was calculated as $\gamma_{ds} = \Delta\delta_{h,ds}/H_{ds}$ (after the definition of Knappett and Craig, 2012) where H_{ds} is the initial specimen thickness. From the corrected data, ϕ_{ds} was calculated using:

$$\phi_{ds} = \tan^{-1}\left(\frac{\tau}{\sigma'_n}\right) \quad (3)$$

The maximum dilation angle in direct shear tests (ψ_{ds}) was calculated using:

$$\psi_{max,ds} = \tan^{-1}\left(\frac{-\Delta\delta_{v,ds}}{\Delta\delta_{h,ds}}\right) \quad (4)$$

4.2.3 Direct shear results

The relation between τ/σ'_n and $\delta_{h,ds}$ is reported for eight tests in Figure 4.3 (a). All tests exhibit a peak value of τ/σ'_n, and diminish to a nearly constant value (τ/σ'_n= 0.65 ± 0.05) at $\delta_{h,ds}$ = 5 mm, with the exception of the tests at σ'_n= 4 and 11 kPa which attain a value of $\tau/\sigma'_n \approx 0.75$ and $\tau/\sigma'_n \approx 0.8$ respectively, at large displacement. The peak stress ratio τ/σ'_n occurs at a horizontal displacement that is consistent with the maximum dilatancy rate (see Figure 4.3 (b)). Moreover, a nearly constant τ/σ'_n is consistent with shearing at constant volume at large displacement. The results indicate that, the lower the applied value of σ'_n, the higher the peak of τ/σ'_n and the greater the increase of $\delta_{v,ds}$. Furthermore, the lower the applied σ'_n, the smaller the $\delta_{h,ds}$ at which the peak value of τ/σ'_n occurs.

Similar results were obtained by testing the sand twice at σ'_n = 51 kPa, for which the specimens were reconstituted to Dr = 53 and 56 %. The denser specimen exhibits, as expected, a slightly

higher peak of τ/σ'_n than that with Dr = 53 %. Also, the denser specimen reached the peak τ/σ'_n at a smaller value of $\delta_{h,ds}$ than the slightly looser specimen, and exhibits a slightly larger value of $\delta_{v,ds}$. In general, an overall good repeatability was observed: given a difference in relative density of 3 %, there is a difference in peak τ/σ'_n of 2 %, and a difference in $\delta_{h,ds}$ at peak τ/σ'_n of 17 %.

4.3 Triaxial tests

Principal stresses in triaxial conditions are represented as σ'_1, σ'_2 and σ'_3 for the major, intermediate and minor principal stresses respectively. The equivalent strains are $\varepsilon_1, \varepsilon_2$ and ε_3. For triaxial compression the stress conditions are $\sigma'_1 > \sigma'_2 = \sigma'_3$ and for simplicity the confining stress ($\sigma'_2 = \sigma'_3$) is termed σ'_3. Strains conditions are $\varepsilon_1 \neq 0$ and $\varepsilon_2 = \varepsilon_3 \neq 0$.

A special triaxial apparatus developed for the SRL was used at NGI. A Humboldt load frame was used for shearing the specimen. The force was measured using one of two different external Interface force transducers: a capacity 0.5 kN (Model SM S/N 605377) for cell pressures σ'_3 < 50 kPa, and a 5 kN capacity (Model SM S/N 018) for $\sigma'_3 \geq$ 50 kPa. A frictionless GCTS-2MPa-cell with an air-bushing system was used. Displacements were measured using a LVDT (RDP-Electronics type: ACT10000, S/N: 153968, to ± 0.001 mm). Pore water pressure was measured using a Druck differential pressure transducer (Unik 5000 Premium, 0 to 20 bar, S/N 3498723). NGI manufactured the cell pressure control unit, null indicator, backpressure burettes and pressure distribution panel. GDS pressure controllers were used to measure and record any volume change (water volume entering or leaving the specimen to compensate for change in volume of the specimen) after a technique developed by Bishop & Henkel (1978). GDS pressure controllers were also used to maintain σ'_3 constant during most, but not all of the triaxial tests.

Therefore, the accuracy and capability of the pressure controllers was extremely important. The GDS advanced pressure controller gave a better resolution and accuracy (σ'_3 ± 1 kPa) at lower stresses ($\sigma'_3 \leq$ 50 kPa) than the GDS standard pressure controller (σ'_3 ± 2 kPa). At very low stresses ($\sigma'_3 \leq$ 11 kPa), tests were performed with a Bishop-type backpressure burette instead of the GDS controller. The burette was considered the most effective device for controlling σ'_3, since a variability of less than ± 1 kPa was achieved. In tests using the backpressure burette all measurements (namely: force, displacement, volume change, cell pressure and pore water pressure) were manually recorded.

4.3.1 Soil reconstitution and testing procedure

Each triaxial specimen was 72 mm in diameter and 144 mm in high (see Figure 4.1(b) and Figure 4.2(b)). The specimen was reconstituted using the under-compaction moist tamping technique after Ladd (1978). The water content of the sand was typically 5 % and the chosen under-compaction factor (U_1) was 0.04, which is typical for reconstituting sands at Dr = 50 %. Eight soil layers of identical height were tamped for reconstituting each specimen. A relative density of 46 % < Dr < 54 % was achieved.

After reconstituting the specimen and sealing the membrane using O-rings, a vacuum of -20 ± 5 kPa was applied to prevent any disturbance and maintain the initial geometry. After placing the specimen and base pedestal in the triaxial cell, the cell was flooded with water on which a surficial layer of oil was placed. At the top of the triaxial cell, above the oil layer, air pressure provides the cell pressure. A cell pressure of ca. 25 kPa was applied while releasing the vacuum. Subsequently, carbon dioxide (CO_2) was flushed trough the specimen, fittings and hoses. Saturation with de-aired water followed the flushing. A cellpressure of around 700 to 750 kPa

was gradually applied to the specimen, while at the same time backpressure (that was approximately 20 kPa lower) was also applied, yielding isotropic consolidation to σ'_3 = 20 ± 5 kPa. Thereafter, Skempton's B-Value was calculated and testing only continued if the B-Value exceeded 0.95.

Tests at $\sigma'_3 \geq 50$ kPa were sheared at a constant rate of displacement $\dot{\delta}$ = 0.8 mm/min. A lower rate of displacement $\dot{\delta}$ = 0.08 mm/min was used for tests at $\sigma'_3 < 50$ kPa with the objective of significantly improving the opportunity to maintain σ'_3 at a constant value during shearing.

4.3.2 Corrections and calculations

In accordance with standard NGI procedures, several corrections were applied to the raw data. Corrections were applied to the backpressure, consolidation and shearing phases. First, during the backpressure application, the axial displacement of the specimen was monitored to account for changes of specimen geometry. An axial displacement limit of 0.15 mm was established, and if that limit was exceeded (which it was in two tests), a volumetric correction was applied to the initial condition of the specimen. The displacement limit is equivalent to an axial strain limit of approximately 0.1 % (ε_1 = 0.15 mm / triaxial specimen height ≈ 0.1 %), and the volumetric strain $\varepsilon_{v,tx} = 3 \cdot \varepsilon_1$. During consolidation and shearing, σ'_3 and σ'_1 were corrected to account for membrane effects. Therefore, the specific extension modulus (C-Value) of the 0.5 mm thick membrane was determined following NGI procedures, as well as axial and radial membrane strains while reconstituting the specimen. Additionally, σ'_1 was corrected to account for the weight of components of the equipment (namely: the rod of the LVDT, the piston, the top cap, and half of the specimen).

The volumetric strain ($\varepsilon_{v,tx}$) is defined as $\varepsilon_{v,tx} = \Delta V / V_0 = \varepsilon_1 + 2\varepsilon_3$, where ΔV is the volume

change and V_0 is the initial volume. The shear strain (γ_{tx}) was calculated as $\gamma_{tx} = \varepsilon_1 - \varepsilon_3$ (after Vaid & Sasitharan, 1992), and the triaxial friction angle ϕ_{tx} was calculated after Bishop (1966):

$$\phi_{tx} = \sin^{-1}\left(\frac{\sigma'_1 - \sigma'_3}{\sigma'_1 + \sigma'_3}\right) \quad (5)$$

Additionally, the maximum dilation angle (ψ_{tx}) was computed after Vaid & Sasitharan (1992):

$$\psi_{max,tx} = \sin^{-1}\left(-\frac{\Delta\varepsilon_{v,tx}}{\Delta\varepsilon_1 - \Delta\varepsilon_3}\right) \quad (6)$$

4.3.3 Triaxial results

The relation between σ'_1/σ'_3 and ε_1 is reported for eight tests in Figure 4.4 (a). Tests at $\sigma'_3 \leq 11$ kPa exhibit a distinct peak value of σ'_1/σ'_3, which diminishes with increasing ε_1 to a nearly-constant value of $\sigma'_1/\sigma'_3 \approx 5.1$ at ε_1= 5 %. In contrast, all other tests exhibit a maximum, rather than peak value of σ'_1/σ'_3 that diminishes to a nearly-constant value of $\sigma'_1/\sigma'_3 \approx 4.2$ at ε_1= 5 %. The lower the cell pressure σ'_3, the higher the peak (or maximum) value of σ'_1/σ'_3 and also the smaller the axial strain ε_1 at which the peak of σ'_1/σ'_3 occurs. Although the stress ratio, σ'_1/σ'_3 tends to a constant value at large displacement, dilation appeared to be still ongoing (Figure 4.4 (b)), which implies the shearing action does not occur at constant volume. Comparison of the shear and deformation response of the specimens indicates that the peak or maximum stress ratio σ'_1/σ'_3 occurs at a ε_1, which is consistent with the maximum dilatancy rate $\left(-\Delta\varepsilon_{v,tx}/\Delta\varepsilon_{1,tx}\right)_{max}$.

Similar results were obtained by testing the sand twice at $\sigma'_3 \approx 100$ kPa, for which the specimens were reconstituted to Dr = 54 and 47 %. The denser specimen exhibits, as expected, a slightly higher peak of σ'_1/σ'_3 than that with Dr = 54 %. Also, the denser specimen reached the peak

σ'_1/σ'_3 at a smaller value of ε_1 than the slightly looser specimen, and exhibits a higher value of $\varepsilon_{v,tx}$ at large strains. In general, an overall good repeatability was observed, given the difference in relative density of 7 %, there is a difference in peak σ'_1/σ'_3 of 2 % , and a difference in ε_1 at peak σ'_1/σ'_3 of 10 %.

4.4 Plane-strain tests

For plane-strain conditions $\sigma'_1 > \sigma'_2 > \sigma'_3$, and ε_1 and $\varepsilon_3 \neq 0$, while $\varepsilon_2 = 0$. The same equipment that was used in the triaxial tests was used for performing the plane-strain tests, with the exception of the cell, top cap, specimen mount and base pedestal assembly. The cell used for the plane-strain tests was a 2MPa-NGI-cell with rotating-bushing system, which is considered to provide a frictionless resistance to axial loading. To impose plane-strain conditions on the specimen, it is constrained by parallel smooth stainless steel plates (see Figure 4.1(c) and Figure 4.2(c)). It should be noted that, in contrast to some plane-strain devices (Kjellman, 1936; Wood, 1958; Cornforth, 1964; Campanella & Vaid, 1973; Mitchell, 1973; El-Nasrallah, 1976; Barden et al., 1969; Finno et al., 1996, 1997; Alshibli & Williams, 2005; Wanatowski 2005), the plane-strain device used in this investigation is not capable of measuring σ'_2. Nevertheless, it was considered sufficiently adequate for the purposes of this investigation.

4.4.1 Soil reconstitution and testing procedure

The plane-strain specimens were 35 mm thick, 70 mm wide and 90 mm high (see Figure 4.1(c) and Figure 4.2(c)), assuring a length/width ratio of 2.0. Sand was reconstituted using the same moist tamping technique of under compaction as previously described for the triaxial tests.

4.4.2 Corrections and calculations

Given the similarity of triaxial and plane-strain procedures and testing, such as backpressure-saturation, consolidation and shearing, standard NGI corrections were also applied to the raw plane-strain data. The standard NGI corrections assume a circular specimen, hence an equivalent circular area was determined for the rectangular specimen, and the corrections in plane-strain testing were applied in an identical way as in triaxial testing. The rationale for adopting this approach was that at small strain values, the peak friction angle is not significantly influenced by underlying assumption in those corrections. More specifically, membrane corrections were applied to obtain σ'_3 and σ'_1, and additionally to calculate σ'_1 to account for the weight of components of the equipment. During the backpressure application, the same axial displacement limit of 0.15 mm for volumetric correction, as in triaxial testing, was adopted. However, the axial strain limit was different to that of the triaxial condition, namely 0.17 %, because of the different specimen high (ε_1 = 0.15 mm / specimen height plane-strain $\approx$ 0.17 %), and the volumetric strain in plane-strain conditions were calculated assuming that $\varepsilon_1 = \varepsilon_3$ while $\varepsilon_2 = 0$. However, only one tests was volumetrically corrected.

Unique to the plane-strain device is the need to correct for adhesion between the greased membrane and the steel plates used to maintain $\varepsilon_2 = 0$. This adhesion has a direct influence in the calculated value of σ'_1. Wood (1958), Blight (1963), Cornforth (1964), Duncan and Seed (1966) and Vaid (1968) have all reported a coefficient of friction between steel and grease due to adhesion around $\mu \approx 0.02$. In the current study, adhesion was found to be around $\mu \approx 0.02$ for $\sigma'_3 \geq 100$ kPa, and $\mu \approx 0.03$ for smaller confining stresses $\sigma'_3 \leq 50$ kPa. The magnitude of the adhesion was obtained by index shear tests in a slightly modified direct shear apparatus on an interface between a greased membrane and steel plates.

Considering any changes of the three major principal stresses, the calculation of ϕ_{ps} should ideally take into account the actual stress path in terms of octahedral stresses ($\sigma'_{oct} = \frac{\sigma'_1+\sigma'_2+\sigma'_3}{3}$). However, since in the current study σ'_2 was unknown, ϕ_{ps} was calculated, as many other research studies (Finn & Mittal (1964), Marachi et al. (1981), Bolton (1986), Oda (1978), Desrues (1984), Alabdullah (2010), amongst others), using the Mohr-Coulomb failure criterion shown in equation (5). Using this assumption, the calculated values of ϕ_{ps} are expected to be up to 10 % smaller than the values that would otherwise be obtained if σ'_2 was known (Alshibli & Williams, 2005).

The volumetric strain in plane-strain is defined as $\varepsilon_{v,ps} = \Delta V/V_0 = \varepsilon_1 + \varepsilon_3$, and the shear strain ($\gamma_{ps}$) is defined as $\gamma_{ps} = \varepsilon_1 - \varepsilon_3$. The plane-strain maximum dilation angle (ψ_{ps}), was calculated after Vaid & Sasitharan (1992):

$$\psi_{max,ps} = \sin^{-1}\left(-\frac{\Delta\varepsilon_{v,ps}}{\Delta\gamma_{ps}}\right) \quad (7)$$

4.4.3 Plane-strain results

The Skedsmo sand exhibited a similar response to loading in plane-strain as that which occurred in triaxial loading. The relation between σ'_1/σ'_3 and ε_1 is reported for eight tests in Figure 4.5 (a). All tests at $\sigma'_3 \geq 25$ kPa exhibit a peak value of σ'_1/σ'_3, which diminishes with increasing ε_1 to a nearly-constant value of $\sigma'_1/\sigma'_3 \approx 4.0$ when $\varepsilon_1 = 5$ %. In contrast, tests at σ'_3 = 12 and 4 kPa diminish to a value of $\sigma'_1/\sigma'_3 \approx 5$ and 7 respectively. The lower the cell pressure σ'_3, the higher the peak (or maximum) of σ'_1/σ'_3 and also the smaller the axial strain ε_1 at which the peak value of σ'_1/σ'_3 occurs. The displacement to peak stress ratio, σ'_1/σ'_3 is consistent with that to maximum dilation of the sand. However, the stress ratio σ'_1/σ'_3 tends to nearly-constant

value at large displacement, even though dilation appeared to be still ongoing in some of the specimens (see Figure 4.5 (b)). Volumetric strain increased steeply in tests at $\sigma'_3 \leq 50$ kPa, reaching a plateau and then continuing to increase gradually with increasing $\varepsilon_{1,ps}$. This observation is distinctive in plane-strain results and was observed neither in direct shear nor in triaxial tests. Comparison of the shear and deformation response of the specimens indicates that the peak or maximum stress ratio σ'_1/σ'_3 occurs at a value of ε_1 that is consistent with the maximum dilatancy rate ($-\Delta\varepsilon_{v,tx}/\Delta\varepsilon_{1,tx}$).

Similar results were obtained by testing the sand twice at $\sigma'_3 \approx 200$ kPa, for which the specimens were reconstituted to Dr = 58 and 55 %. The denser specimen exhibits, as expected, a slightly higher peak of σ'_1/σ'_3 than that with Dr = 55 %. Also, the denser specimen reached the peak of σ'_1/σ'_3 at a smaller value of ε_1 than the slightly looser specimen, and exhibits a higher value of $\varepsilon_{v,ps}$ at large strains. In general, an overall good repeatability was observed by comparing the two tests at $\sigma'_3 \approx 200$ kPa, given the difference in relative density of 3 %, there is a difference in peak σ'_1/σ'_3 of 1 % and a difference in ε_1 at peak σ'_1/σ'_3 of 2 %.

4.5 Analysis and discussion of experimental results

A synthesis of the experimental results is given herein, together with a comparison of the Skedsmo sand with empirical relations and the findings of other studies on the strength of sands. For simplicity, only the term peak friction angle is used in reference the peak and maximum strength alike.

4.5.1 Variation of peak friction angle of Skedsmo sand

A comparison of the results in terms of peak friction angle (ϕ_p), maximum dilation angle (ψ_{max})

and dilatancy rate ($(\Delta\varepsilon_v/\Delta\varepsilon_1)_{max}$) is given in Figure 4.6. The magnitude of $\phi_{p,ps}$ increases by as much as 20º when σ'_3 decreases from 300 to 4 kPa, see Figure 4.6 (a). Likewise $\phi_{p,ds}$ and $\phi_{p,tx}$, which are similar magnitude, increase by as much as 11º with decreasing σ'_n or σ'_3, respectively, from 300 to 4 kPa. In all the cases the relation of ϕ_p with the logarithm of effective stresses is inferred as linear and inversely proportional. The trend of decreasing ϕ_p with increasing stress is toward a common value at $\sigma'_n \approx \sigma'_3 \approx 300$ kPa. In contrast, the values of $\phi_{p,ps}$ are consistently larger than $\phi_{p,tx}$ and $\phi_{p,ds}$ at $\sigma'_3 \leq 200$ kPa. The finding that $\phi_{p,ps}$ exceeds $\phi_{p,tx}$ is consistent with that reported by Cornforth (1964), Lee & Seed (1967), Marachi et al. (1981), Boyle (1995) and Hanna (2001). Furthermore, Rowe (1969) and Boyle (1995) report that $\phi_{p,ps}$ exceeds $\phi_{p,ds}$.

All three devices establish an increase of ψ_{max} with decreasing effective stress (see Figure 4.6 (b)). Inspection shows the values of $\psi_{max,ps}$ and $\psi_{max,tx}$ are very similar, and increase from approximately 8º at $\sigma'_3 \approx 300$ kPa to 30º at $\sigma'_3 \approx 4$ kPa. The values of $\psi_{max,ds}$, which increase from approximately 8º to 15º when σ'_3 decreases from 300 to 4 kPa, are significantly lower than the maximum dilation angle in plane-strain ($\psi_{max,ps}$ = 4º to 26º) and triaxial ($\psi_{max,tx}$ = 8º to31º) loading. However, the trend of decreasing ψ_{max} with increasing effective stress is toward a common value at $\sigma'_n \approx \sigma'_3 \approx 300$ kPa.

A stress-dependent dilatancy rate ($(\Delta\varepsilon_v/\Delta\varepsilon_1)_{max}$) was found in the results from all three devices (see Figure 4.6 (c)). The magnitude of the dilatancy rate in plane-strain conditions ($(\Delta\varepsilon_v/\Delta\varepsilon_1)_{max,ps}$) increases by a value of up to 1.6 when σ'_3 decreases from 300 to 4 kPa. In contrast, the magnitude of the dilatancy rate in triaxial conditions ($(\Delta\varepsilon_v/\Delta\varepsilon_1)_{max,tx}$) increases to a value of 1.0 over the same stress range, and that in direct shear conditions ($(\Delta\varepsilon_v/\Delta\varepsilon_1)_{max,ds}$)

increases to a value of 0.8. Values of $(\Delta\varepsilon_v/\Delta\varepsilon_1)_{max,ps}$ are consistently higher than $(\Delta\varepsilon_v/\Delta\varepsilon_1)_{max,tx}$, which in turn are consistently higher the $(\Delta\varepsilon_v/\Delta\varepsilon_1)_{max,ds}$ at $4 < \sigma'_n \approx \sigma'_3 <$ 300 kPa. Once again, the trend of decreasing $(\Delta\varepsilon_v/\Delta\varepsilon_1)_{max}$ with increasing stress is toward a common value at $\sigma'_n \approx \sigma'_3 \approx 300$ kPa.

The increasing values of ϕ_p in Skedsmo sand with decreasing confining stresses in all three devices, as well as the relative differences between the value of $\phi_{p,ps}$ and the values of $\phi_{p,tx}$ and $\phi_{p,ds}$, are attributed to the influence of dilatancy rate. This relative difference of $\phi_{p,ps}$ and $\phi_{p,tx}$ is consistent with prior observations reported by Bolton (1986).

4.5.2 Comparison of the Skedsmo sand with empirical relations

Empirical relations have been published in the literature for both triaxial and plane-strain data. Consider first the triaxial results obtained in the current study. Vaid & Sasitharan (1992) report an empirical relation between $\phi_{p,tx}$, ϕ_{cv} and $\psi_{max,tx}$:

$$\phi_{p,tx} = \phi_{cv} + 0.33 \cdot \psi_{max,tx} \tag{8}$$

It is based on more than 50 triaxial compression and triaxial extension test results, at a stress range of $14 < \sigma'_3 < 2400$ kPa, on a uniformly graded (C_u = 1.8) quartz sand (D_{50} = 0.34 mm), with subrounded particles, called Erksak sand.

A best-fit line through the constant volume friction angle (ϕ_{cv}= 33 ± 1º at ψ_{max} = 0) of Skedsmo sand and the triaxial data ($\phi_{p,tx}$ and $\psi_{max,tx}$) of the current study is plotted in Figure 4.7. The best-fit line was considered for an effective stress $\sigma'_3 \geq 25$ kPa, to allow for a direct comparison with the Vaid & Sasitharan relation. The empirical relation obtained for the Skedsmo sand triaxial data is given by:

$$\phi_{p,tx} = \phi_{cv} + 0.43 \cdot \psi_{max,tx} \quad (9)$$

It is similar to Vaid & Sasitharan's relation. The agreement between the two empirical relations appears reasonable, given the nature of the two sands.

Consider now the plane-strain results obtained in the current study. Based on a database of plane-strain compression tests on different sands at effective stresses σ'_3 > 50 kPa, Bolton (1986) proposed an empirical relation between $\phi_{p,ps}$, ϕ_{cv} and $\psi_{max,ps}$:

$$\phi_{p,ps} = \phi_{cv} + 0.8 \cdot \psi_{max,ps} \quad (10)$$

A best-fit for the plane-strain data obtained in the current study, for tests at $\sigma'_3 \geq 50$ kPa, is given by:

$$\phi_{p,ps} = \phi_{cv} + 0.9 \cdot \psi_{max,ps} \quad (11)$$

The relation for the current plane-strain data is similar to Bolton's relation. The agreement between the two empirical relations appears reasonable, and further strengthens the confidence in the results of the laboratory strength tests on Skedsmo sand.

4.5.3 Comparison of the Skedsmo sand with other sands

Bishop (1966) stated, based on the experimental work of Cornforth (1961) on Leighton-Buzzard sand, that the axial strain required to mobilized $\phi_{p,ps}$ varied between approximately 1 % for dense sand, 2 % for medium dense sand, and 4 % for loose sand. This understanding is embodied in the BS-8006, which states that the peak plane-strain friction angle should be used in design of reinforced soil retaining structures because of the small strains of approximately 1 % measured in instrumented structures. The current plane-strain results suggest that the axial strain to mobilize $\phi_{p,ps}$ is highly stress-dependent, particularly at very low stresses. The axial strain to

reach the peak plane-strain strength of Skedsmo sand ranged between 0.5 % < ε_1 < 2.5 %, for a cell pressure between 4 and 300 kPa, respectively, for the medium dense specimens examined in testing.

Very few sands have been comprehensively tested under all three conditions of direct shear, triaxial and plane-strain loading. Indeed at low stresses, a comparison of strength values in these three conditions is seldom available. Boyle (1995) presented one of the few databases of strength, in terms of $\phi_{p,ps}$, $\phi_{p,tx}$ and ϕ_{ds} for the angular Rainier sand (see Table 4.1), which is similar to the very angular Skedsmo sand (see Figure 4.8). Peak friction angles of Rainier sand are, in all three devices, larger than those for Skedsmo sand. The difference is attributed primarily to a higher value of relative density ($Dr \approx$ 90 %) at which Rainier sand was reconstituted, compared to that of Skedsmo sand in the current study ($Dr \approx$ 52 %). However, the increase of $\phi_{p,ps}$ with decreasing effective stress of both sands is comparable in magnitude. The relative position of $\phi_{p,ps}$with respect to $\phi_{p,tx}$ and $\phi_{p,ds}$ reported earlier for the Skedsmo sand appears to be in reasonable agreement with that observed for Rainier sand. Additionally, for both sands, the peak strength in triaxial and direct shear is similar ($\phi_{p,tx} \approx \phi_{p,ds}$).

The $\phi_{p,ps}$ data of Figure 4.8 are reproduced together with three other sands from the studies of Boyle (1995), Riemer (1999) and Alabdullah (2010). Detailed information on the sands is given in Table 4.1. A highly-stress dependent response of $\phi_{p,ps}$ is observed for all of the sands (see Figure 4.9). Moreover, the angular sands (Rainier and Skedsmo sand) mobilize larger values of $\phi_{p,ps}$ in comparison with the sub-angular sand (Hostun sand), which in turn shows a larger value of $\phi_{p,ps}$ than the rounded sands (Ottawa or RMC sand). This comparison yields further confidence in the plane-strain results of the current study.

4.6 Summary and conclusions

From the advanced shear strength tests on the backfill sand of the Norwegian structure, in plane-strain, triaxial and direct shear conditions, in the general stress range $4 \leq \sigma'_3$ or $\sigma'_n \leq 300$ kPa, the following conclusions are drawn:

- Sufficient high quality shear strength data were obtained from the experimental program. However, testing at low stresses (≤ 5 kPa) in triaxial and plane-strain conditions proves a challenge, primarily due to the difficulties of maintaining σ'_3 constant during the shearing process.
- The peak friction angle (ϕ_p) in all testing conditions (plane-strain, triaxial and direct shear) shows a stress dependency, which diminishes with decreasing stress to a common value of ϕ_p at σ'_3 = 300 kPa. The increase of the peak friction angle in the plane-strain condition is almost 20º, while in triaxial and direct shear conditions it is around 10º, when stress (σ'_n or σ'_3) decreases from about 300 to 4 kPa. The peak plane-strain friction angle ($\phi_{p,ps}$) is higher than the triaxial friction angle ($\phi_{p,tx}$), which in turn is similar to the peak direct shear friction angle ($\phi_{p,ds}$). This can be expressed as: $\phi_{p,ps} > \phi_{p,tx} \approx \phi_{p,ds}$.
- Plane-strain and triaxial tests results are in good agreement with the empirical relation of Vaid & Sasitharan (1992) and of Bolton (1986). This finding suggests that the tests results in both configurations are credible.
- The strength data from Skedsmo sand seem to be in good agreement with the few available plane-strain data for other sands. Specifically, the stress dependency of $\phi_{p,ps}$ at low stress is comparable with the limited published data on four other sands.

Table 4.1 Published data of tested sands at low stresses ($\sigma'_3 < 50$ kPa)

Reference	Sand name	Shape	Cu	Cc	d_{50} (mm)	d_{10} (mm)	e_{min} (-)	e_{max} (-)	Dr (%)	ϕ_{cv} (°)	Size of plane-strain specimen (mm), $T \cdot W \cdot H$*	Reconstitution technique
Current study	Skedsmo	Very angular	2.6	1.3	0.20	0.11	0.50	0.88	52	35±1	35 · 70 · 90	Moist tamping
Alabdullah (2010)	Hostun	Angular to sub-angular	1.7	1.1	0.36	0.21	0.66	0.89	100	36	40 · 100 · 120	Dry and water pluviation
Riemer (1999)	RMC	Rounded	1.1	2.3	0.34	0.30	n/a	n/a	50	33±1	n/a	n/a
Boyle (1995)	Ottawa	Rounded	1.6	1.0	0.26	0.17	0.51	0.75	90	35	n/a	Dry tamping
Boyle (1995)	Rainier	Angular (gravelly sand)	4.1	1.0	0.55	0.21	0.46	0.76	90	n/a	n/a	Moist tamping

* T = thick, W = wide, H = high

(a)

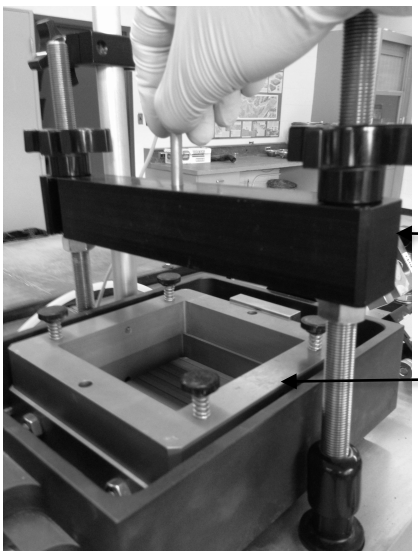

(b) (c)

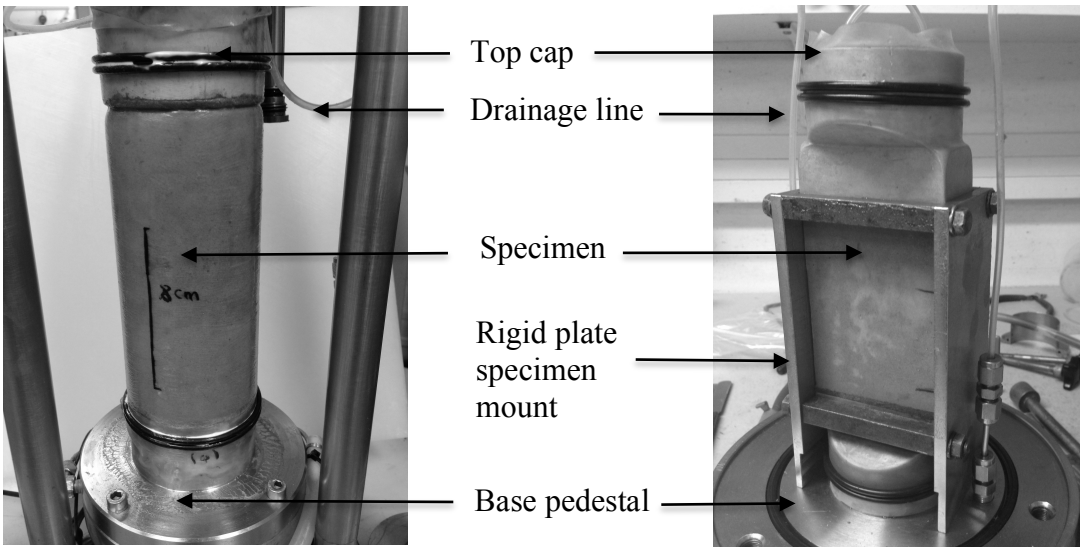

Figure 4.1 Photos of equipment: (a) direct shear box (b) triaxial and (c) plane-strain

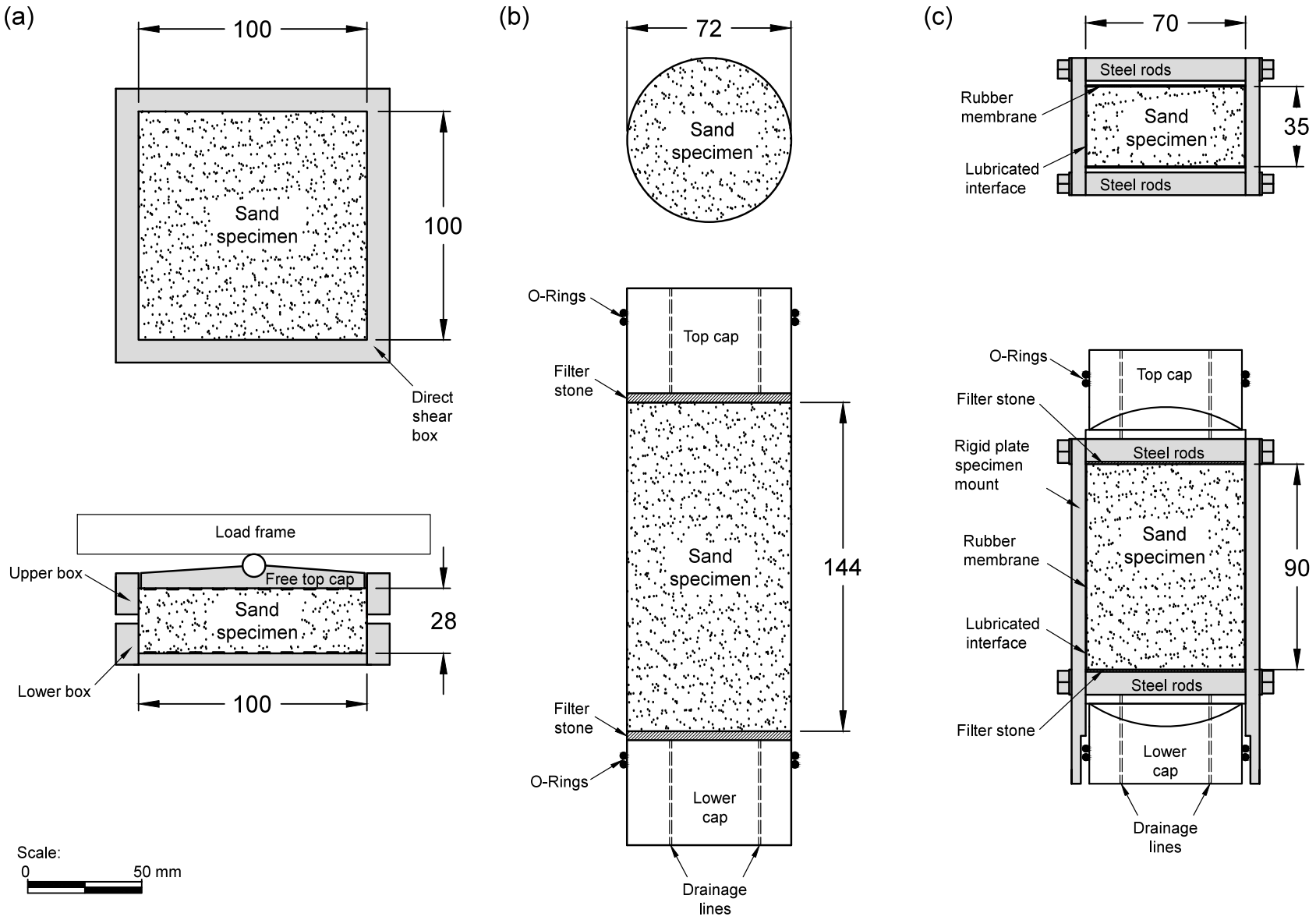

Figure 4.2 Schematic drawing of the test specimen in plan view and cross-section: (a) direct shear (b) triaxial and (c) plane-strain

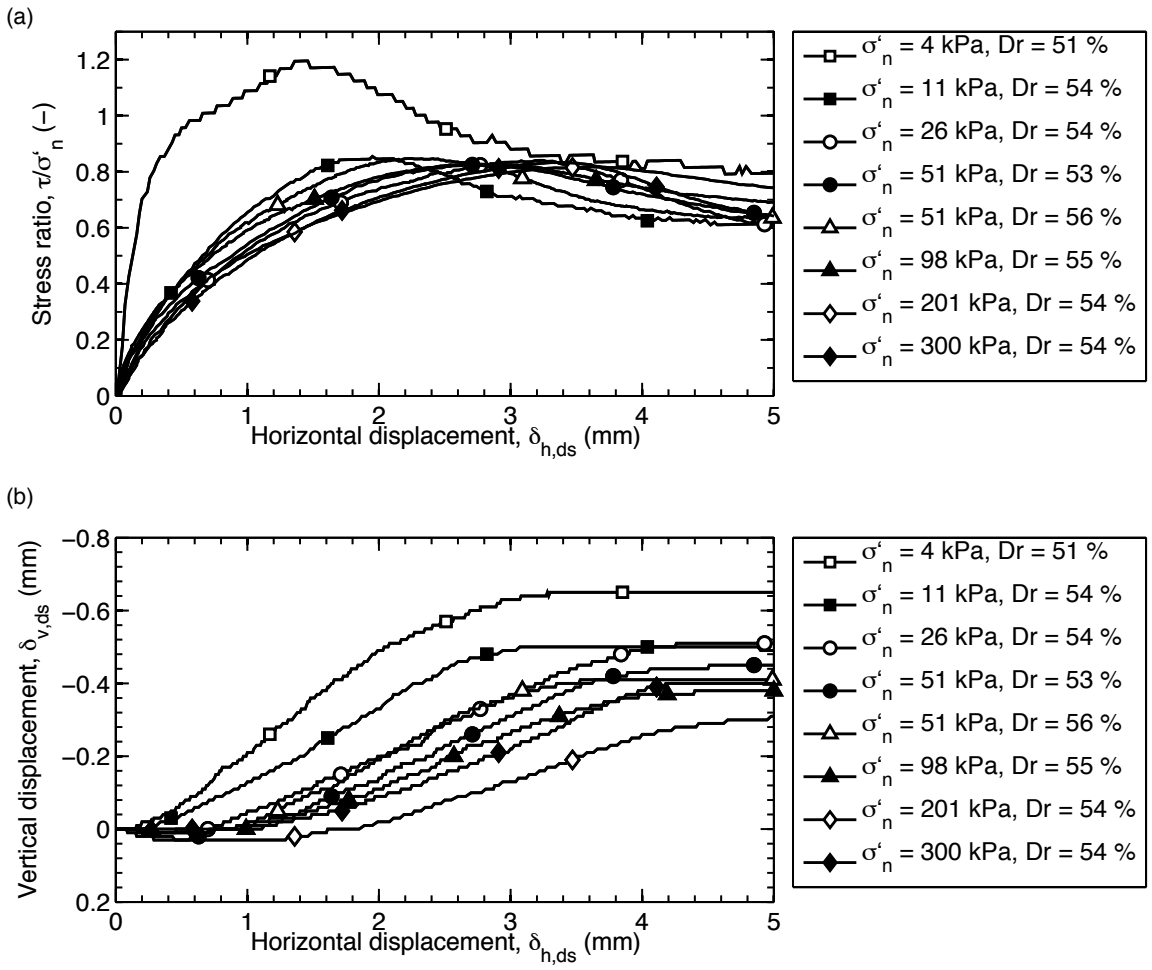

Figure 4.3 Direct shear tests: (a) stress ratio and (b) vertical vs. horizontal displacement

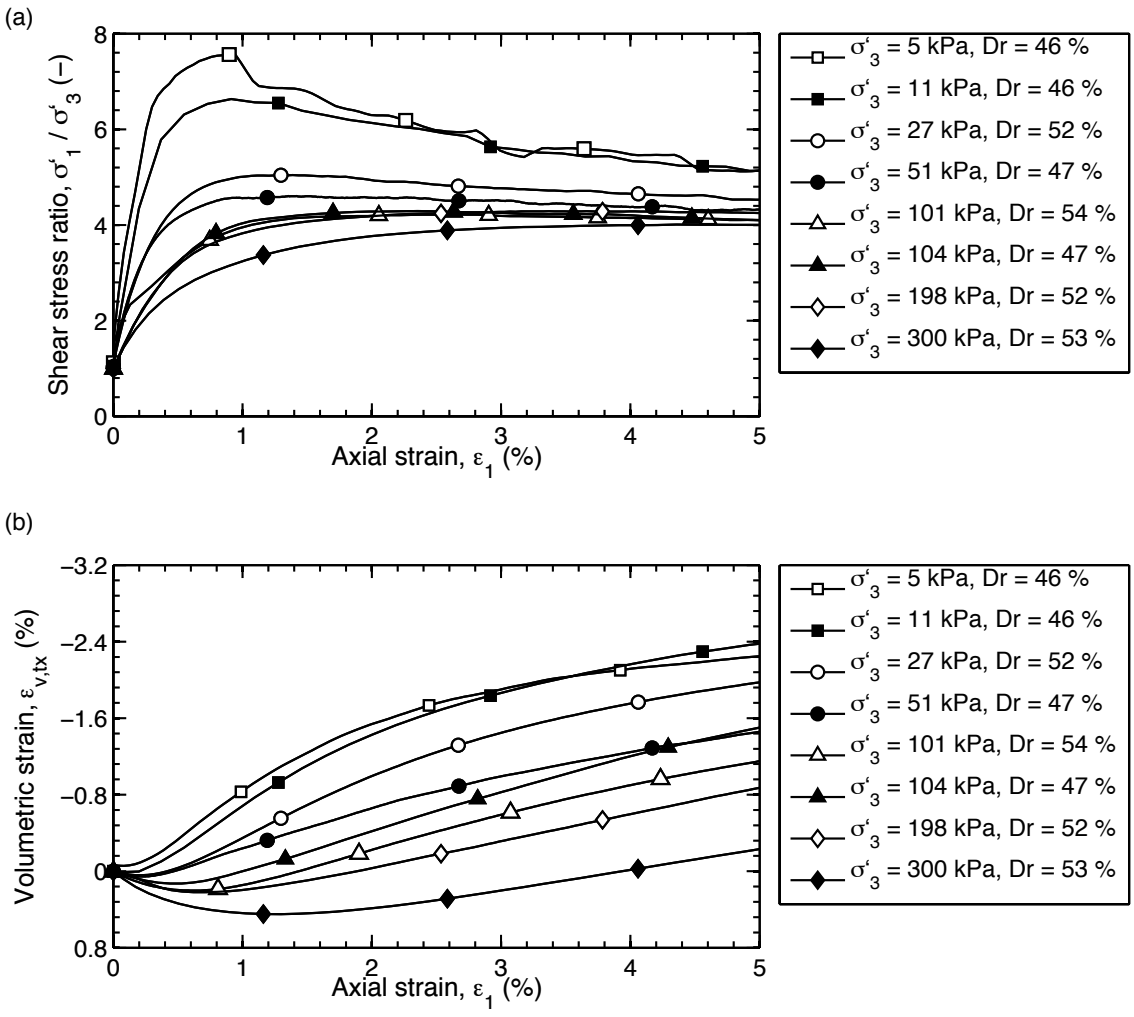

Figure 4.4 Triaxial tests: (a) shear stress ratio and (b) volumetric strain vs. axial strain

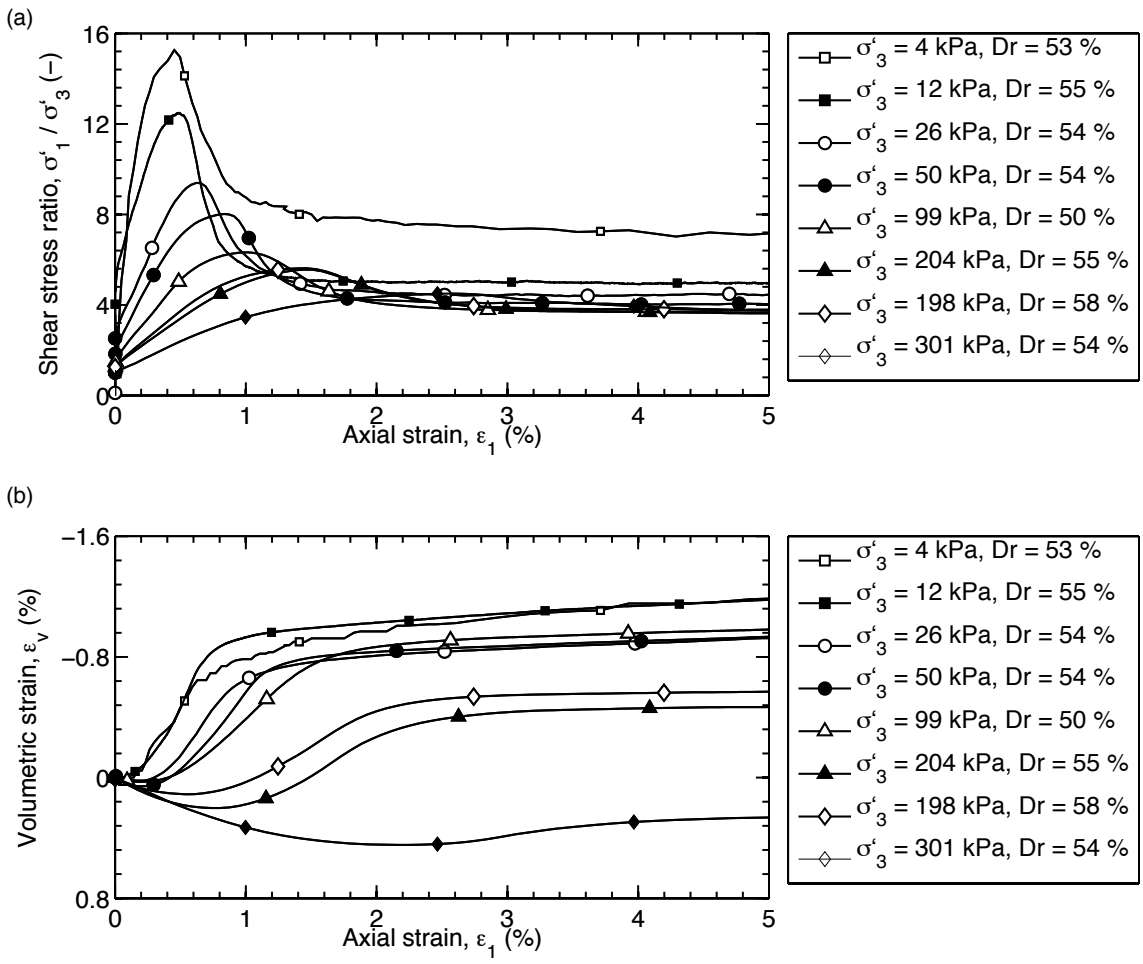

Figure 4.5 Plane-strain tests: (a) shear stress ratio and (b) volumetric strain vs. axial strain

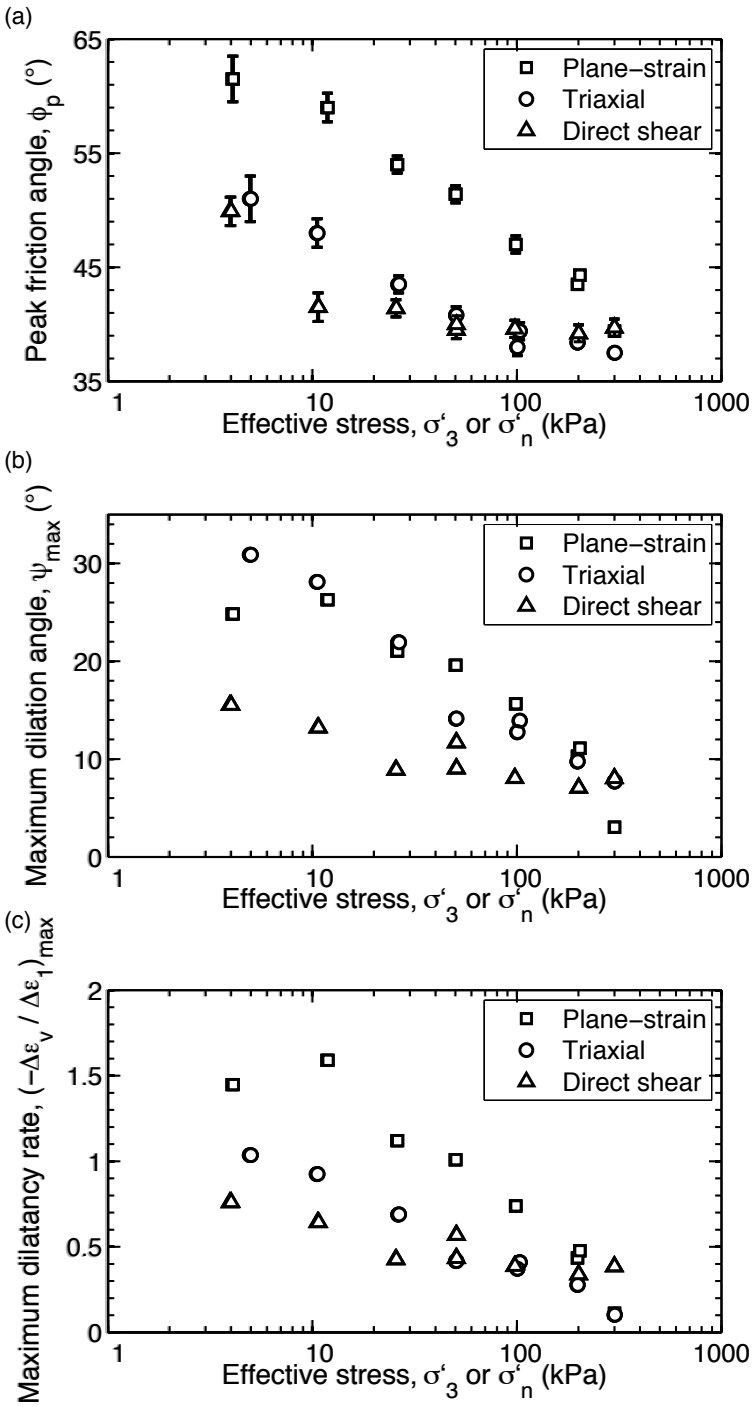

Figure 4.6 Comparison of plane-strain, triaxial and direct shear results: (a) peak friction angle (b) maximum dilation angle and (c) rate of dilation

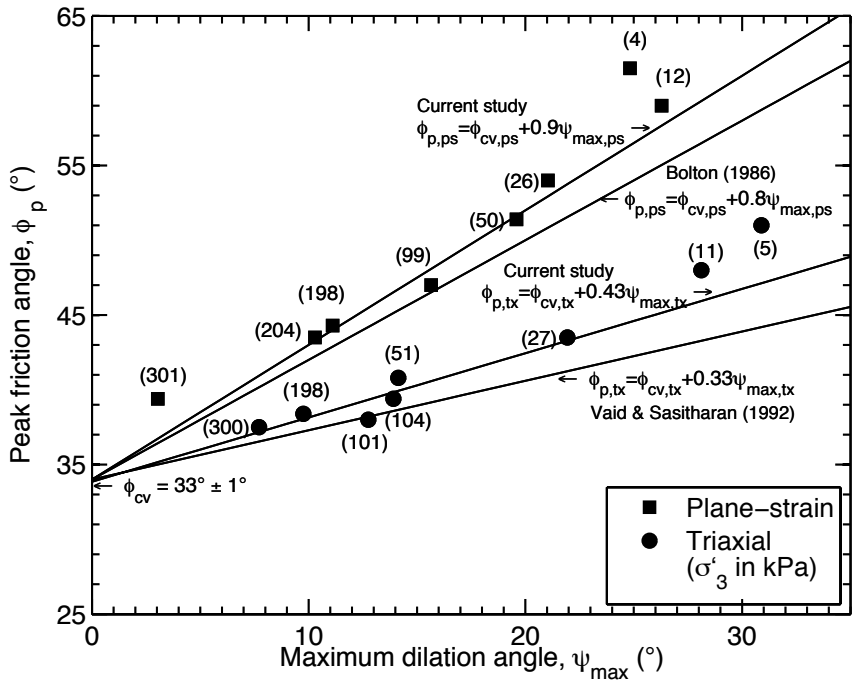

Figure 4.7 Comparison of plane-strain and triaxial results with empirical relations of Vaid & Sasitharan (1992) and Bolton (1986)

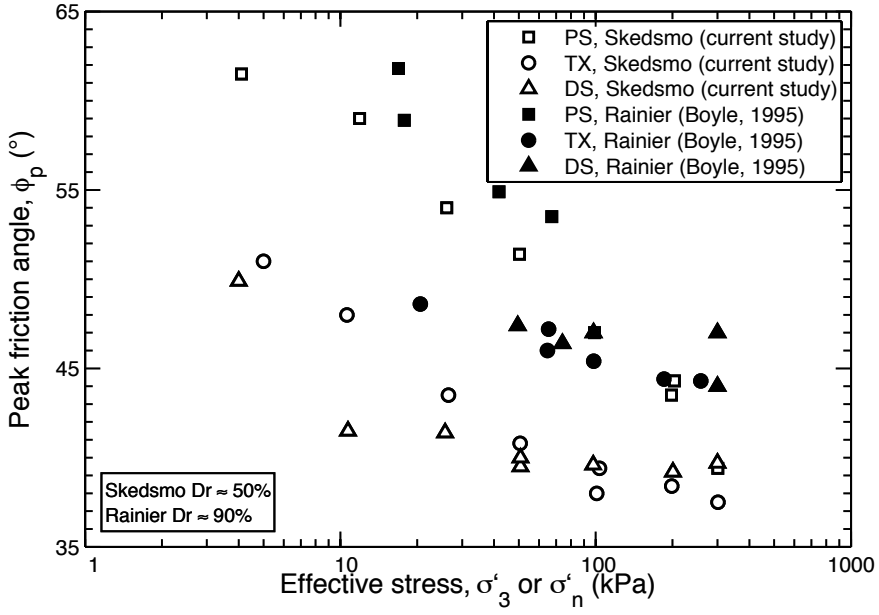

Figure 4.8 Comparison of the $\phi_{p,ps}$, $\phi_{p,tx}$ and $\phi_{p,ds}$ (current study with Boyle, 1995)

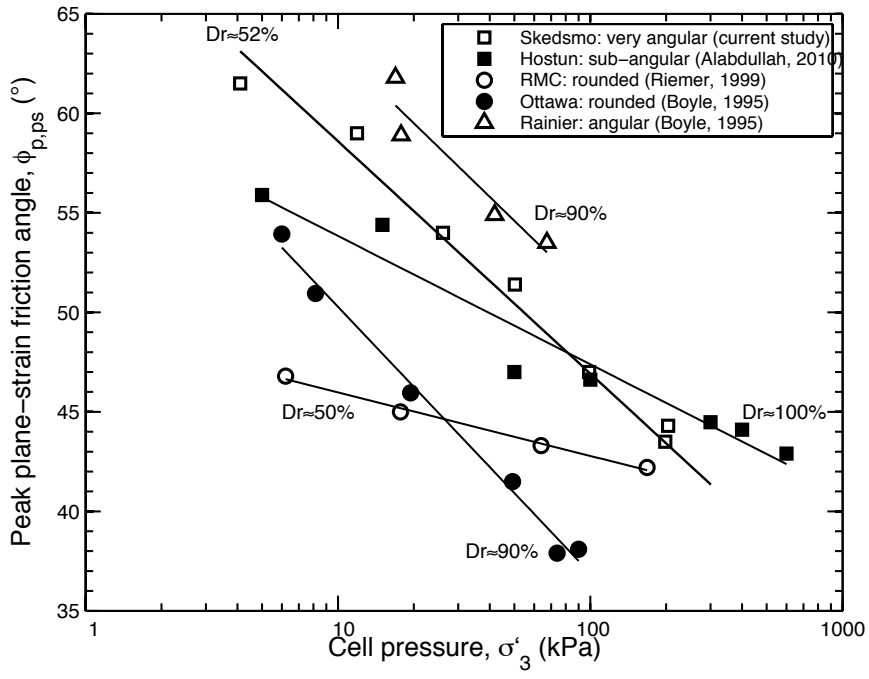

Figure 4.9 Comparison of the $\phi_{p,ps}$ (current study with other studies, see Table 4.1)

5. BACK-ANALYSIS

5.1 Introduction

Design of reinforced soil retaining structures requires an analysis of external and internal stability. An internal stability analysis gives consideration to pullout, structural resistance of the face elements, structural resistance of the face connections, and tensile rupture of the reinforcement. In back-analyzing the Norwegian reinforced soil structure only the consideration of mobilized tensile force in the geogrid reinforcement need be addressed. Codes of practice, such as the American US-FHWA-NHI-10-024 (2009), AASHTO LRFD Bridge Design Specifications (2009) and the British BS-8006 (2010), suggest limit equilibrium methods be used for this purpose. These methods include: a lineal analysis, a bilineal analysis (also known as two-part wedge analysis, mentioned only in BS-8006), a circular or non-circular analysis, a log-spiral failure analysis, the coherent gravity method, and a conjugate stress analysis. However, this study uses the most common methods, namely: lineal and bilineal analyses. Those force-equilibrium analyses are believed to be more appropriate for calculating the tensile force in the reinforcement in the sloped wall structure. Through these analyses, the variation of calculated tensile force per unit width (T_{cal}) with friction angle of the backfill soil was obtained. By comparing T_{cal} with the sum of the mobilized total tensile force in each layer of geogrid reinforcement in Section 'N' of the reinforced soil structure (T_{mob} = 15.3 kN/m, see Table 2.1) the mobilized friction angle (ϕ_{mob}) within the reinforced slope was back-calculated.

5.2 Calculation of tensile force per unit width in design (T_{cal})

The input parameters needed for performing the back-analysis are given in Table 5.1. A schematic illustration of the locus of slip considered in each of the chosen limit equilibrium methods is shown in Figure 5.1.

5.2.1 Lineal slip analysis

In the lineal slip analysis, T_{cal} is obtained by considering the lateral earth pressure coefficient (K_{LS}), the unit weight of the soil (γ) and the height of the reinforced steep slope (H), in the relation:

$$T_{cal} = 0.5 \cdot K_{LS} \cdot \gamma \cdot H^2 \qquad (12)$$

For calculating K_{LS} a simplified version of the Coulomb equation can be used for wall face batters (see AASHTO, 2009). Knowing the slope angle of the face to the horizontal (θ), and the soil friction angle, K_{LS} is obtained from:

$$K_{LS} = \frac{sin^2(\theta + \phi)}{sin^3\theta \left(1 + \frac{sin\,\phi}{sin\,\theta}\right)^2} \qquad (13)$$

The values of K_{LS} and corresponding values of T_{cal} for the lineal slip analysis are reported in Table 5.2.

5.2.2 Bilineal slip analysis

For calculating T_{cal} in the bilinear slip analysis, the same equation as in the linear slip analysis is considered (see Equation (12)). However, the force coefficient in the bilineal analysis (K_{BS}) differs from that in the lineal analysis, and can be obtained using simplified charts after Jewell

(1990, chart 1, appendix 1). The values of K_{BS} and corresponding values of T_{cal} are also reported in Table 5.2.

5.3 Mobilized friction angle (ϕ_{mob}) within the reinforced steep slope

By comparing the sum of the measured tensile force in the geogrid (T_{mob} = 15.3 kN/m) with T_{cal}, a value of mobilized friction angle (ϕ_{mob}) in the backfill soil was obtained (see Figure 5.2). The resulting ϕ_{mob} = 41 ± 1° is believed representative of the shearing resistance developed to achieve equilibrium within the reinforced slope.

5.4 Comparison of ϕ_{mob} with experimentally obtained strength values

The use of stress-strain experimental results to determine appropriate mobilization of strength has been advocated by Bolton (1993; 1996). Therefore, taking into account the principle of strain compatibility, the experimentally-obtained values of ϕ (in direct shear, triaxial and plane-strain conditions at $\sigma'_n = \sigma'_3 = 25$ kPa) are compared with ϕ_{mob} (see Figure 5.3). The laboratory test data are plotted with reference to shear strain (see Chapter 4). The test data at 25 kPa are selected as being generally representative of the expected magnitude of mean effective stress along the postulated locus of slip (see Figure 2.2): shear strain to reach the peak friction angle in plane-strain and triaxial testing is similar (1 < γ_{ps} or γ_{tx} < 3 %), and significantly less than the shear strain in the direct shear tests ($\gamma_{ds} \approx 10$ %).

Since a good interlocking of geogrid and soil was found within the reinforced slope, the geogrid strain is believed equal to the soil strain. Measured strains in the field structure were $\gamma_{mob} \approx 0.5 \pm 0.2$ % (see Table 2.1), and it is believed reasonable to compare this average value with the laboratory shear strain data. Even though the experimental shear strains are not strictly equal to

the geogrid strains, the assumption is made in order to evaluate mobilized conditions within the reinforced slope and is believed reasonable for this purpose. At a shear strain of $\gamma_{mob} \approx 0.5 \pm 0.2$ %, the laboratory data at $\sigma'_n = \sigma'_3 = 25$ kPa yield $\phi_{ps} \approx 46°$, $\phi_{tx} \approx 35°$ and $\phi_{ds} \approx 8°$. The values are reproduced in Figure 5.4, together with an upper and lower bound value for the case of $\gamma_{mob} \approx 0.5 \pm 0.2$ %, and plotted against the back-calculated value of ϕ_{mob} = 41 ± 1°. The close agreement of ϕ_{mob} with ϕ_{ps} suggests, that plane-strain conditions may be prevalent within the reinforced structure. However, from Figure 5.3, it also appears that the magnitude of deformation in the field is insufficient to mobilize fully the peak plane-strain friction angle of the soil ($\phi_{p,ps}$). It should be noted that the companion finding that $\phi_{p,tx} \approx \phi_{p,ds} \approx \phi_{p,mob}$ is believed coincidental.

5.5 Summary and conclusions

From the back-analysis and the comparison of the field and laboratory data, the following conclusions are made:

- Good agreement was found between T_{cal} (FS = 1) and T_{mob} when ϕ_{mob} = 41 ±1°. This friction angle is believed representative of the shearing resistance developed to achieve equilibrium within the reinforced slope.

- ϕ_{mob} is consistent with the experimentally obtained plane-strain friction angle at 25 kPa and a strain of approximately 0.5 %. Therefore, the laboratory testing provides evidence in support of the expectation that plane-strain conditions likely prevail within the reinforced steep slope.

- ϕ_{mob} is coincidentally similar to the experimentally obtained values of peak triaxial and

peak direct shear friction angles at 25 kPa ($\phi_{mob} \approx \phi_{p,tx} \approx \phi_{p,ds}$). However, strains needed to reach $\phi_{p,tx}$ or $\phi_{p,ds}$ are larger and inconsistent with those measured in the reinforced steep slope.

Table 5.1 Parameters for back-analysis

Parameter	Symbol	Unit	Value
Slope height	H	m	4.8
Soil unit weight	γ	kN/m^3	17.0
Friction angle	ϕ	º	20 to 60
Slope batter angle*	θ	º	116.6

* See Figure 5.1

Table 5.2 Variation of T_{cal} with select friction angles

Lineal slip		Bilineal slip	
Force coefficient	Tensile force	Force coefficient	Tensile force
K_{LS}	T_{cal}	K_{BL}	T_{cal}
(-)	(kN/m)	(-)	(kN/m)
0.345	67.7	0.385	75.4
0.174	34.2	0.213	41.7
0.078	14.6	0.091	17.8
0.022	4.3	0.027	5.3

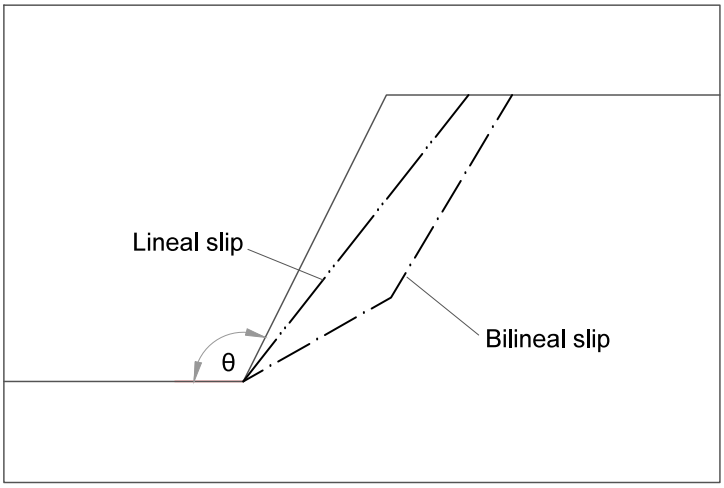

Figure 5.1 Schematic illustration of the locus of slip

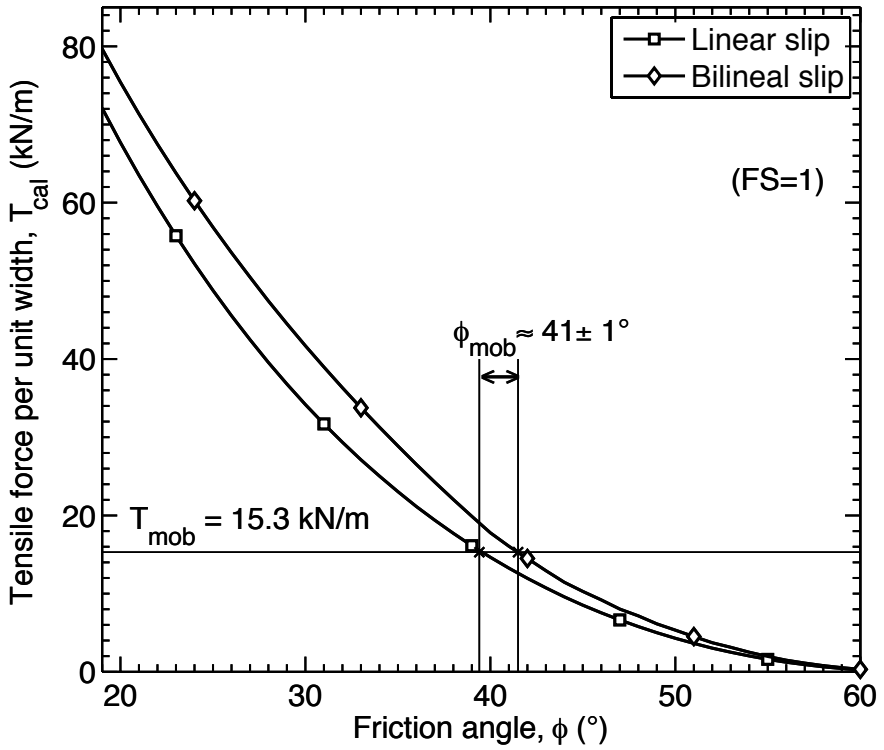

Figure 5.2 Variation of calculated tensile force per unit width (T_{cal}) with friction angle

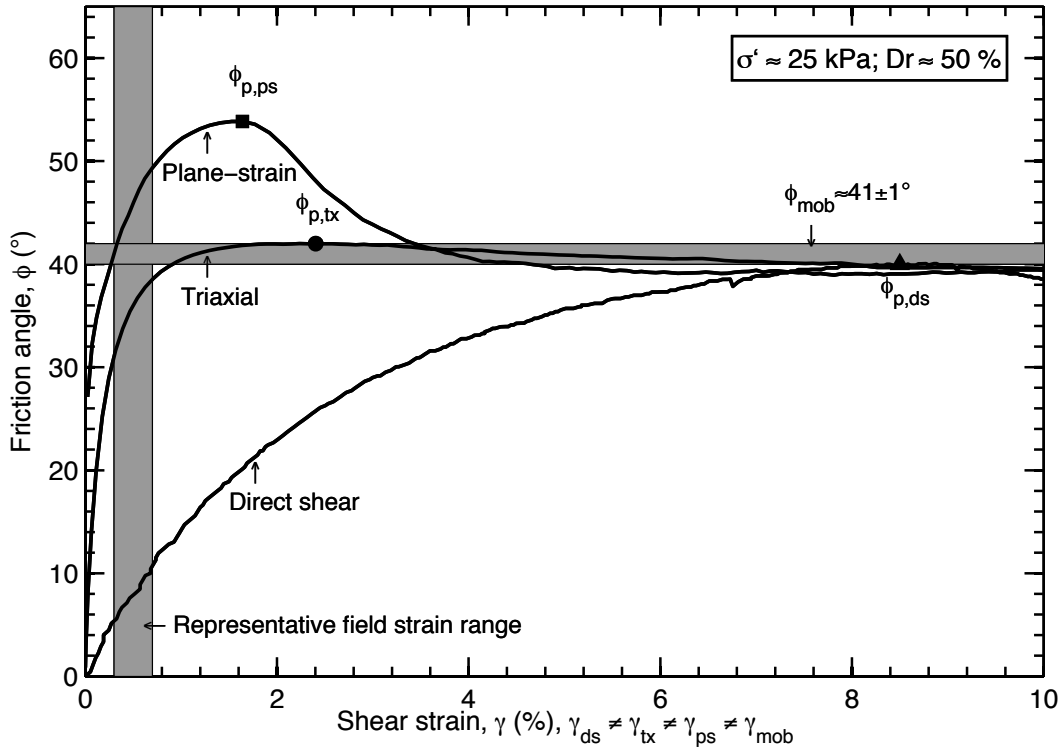

Figure 5.3 Interpretation of mobilized friction angle (note the different shear strains)

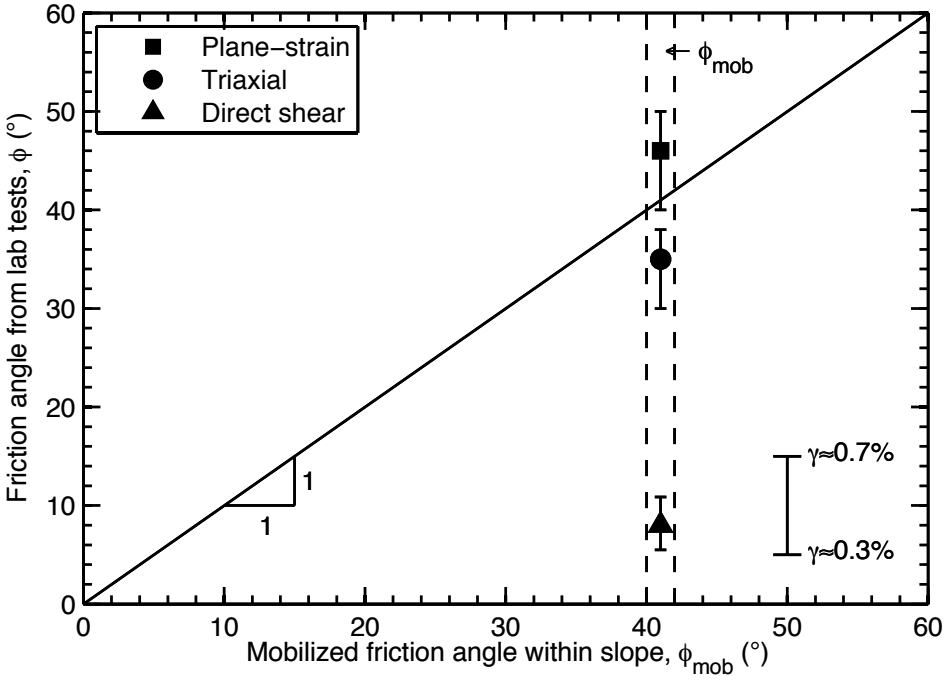

Figure 5.4 Comparison of friction angle from laboratory testing and back-analysis

6. CONCLUSIONS AND RECOMMENDATIONS

The main conclusions of the current research are presented herein, together with recommendations for future work.

6.1 Conclusions on geogrid durability

The durability of exhumed geogrid samples was assessed by visual inspection and a series of index and strength tests. From the evidence obtained it is concluded that:

- The geogrid has experienced no major physical damage, nor significant degradation, after the elapsed time of 25 years of being buried.

6.2 Conclusions on shear strength of the Skedsmo sand

From the strength tests performed in direct shear, triaxial and plane-strain, the following conclusions are drawn:

- The values of peak friction angle in triaxial loading ($\phi_{p,tx}$) seem reasonable in comparison with the empirical relation of Vaid and Sasitharan (1992).
- The values of peak friction angle in plane-strain loading ($\phi_{p,ps}$) are compatible with the empirical relation of Bolton (1986).
- The combined dataset for ϕ_p in all three loading conditions, obtained for the Skedsmo sand, is in good agreement with the few published studies in the literature. More specifically, the trend of the results is very similar to that found in four other sands, for

which $\phi_{p,ps} > \phi_{p,tx} \approx \phi_{p,ds}$. The strength values are significantly stress-dependent at low stresses.

- The peak plane-strain friction angle ($\phi_{p,ps}$), as well as the peak triaxial friction angle ($\phi_{p,tx}$) are mobilized at axial strains between $0.5 < \varepsilon_1$ or $\varepsilon_1 < 2.5$ %.

6.3 Conclusions from back-analysis of the instrumented structure

- Strength testing of the backfill soil, and a consideration of the mobilized friction angle that is informed by a back-analysis of the structure, provide evidence in support of the expectation that plane-strain conditions likely prevail within the reinforced soil steep slope. The belief is founded on an interpretation of the data that assumes the soil strain in the field is comparable to shear strain in the laboratory test devices.
- The mobilized strength within the reinforced slope (ϕ_{mob}) is coincidentally similar to the experimentally obtained values of peak triaxial and peak direct shear friction angles. However, shear strains in the field are not compatible with shear strains to peak in triaxial and direct shear tests.

6.4 Implication of the findings for current design practice

The combination of advanced laboratory strength testing of the backfill soil and companion back-analysis of the unique instrumented reinforced steep slope has the following implications for current design practice:

- BS-8006 assumes that "under plane-strain conditions… the axial strains to mobilize $\phi_{p,ps}$ are small", and consequently "$\phi_{p,ps}$ might be mobilized at axial strains of 1%". The plane-strain data support this assumption, but only for relatively low stresses $\sigma'_3 < 50$

kPa. At higher stresses, the strain to peak is found to be grater than 1%, likely because the axial strains necessary to reach $\phi_{p,ps}$ are not only stress-dependent, but also depend on many other factors, including: particle shape, relative density, mineralogy, grain size and fabric.

- BS-8006 advocates the use of peak plane-strain friction angle ($\phi_{p,ps}$) for designing steep slopes. However, a comparison between ϕ_{mob} and $\phi_{p,ps}$ implies that $\phi_{p,ps}$ has not been mobilized, a finding that is attributed to the phenomenon of strain compatibility in the backfill soil and the geogrid reinforcement. Assuming $\phi_{p,ps}$ for design of the Norwegian reinforced slope, and a factor of safety of FS_R = 1.3, would yield substantially less reinforcement.
- USFHWA and AASHTO advocate the use of $\phi_{p,tx}$ or $\phi_{p,ds}$ in design of reinforced structures. Coincidentally, in this research study $\phi_{p,tx}/\phi_{mob} \approx \phi_{p,ds}/\phi_{mob} \approx 1$. Given that $\phi_{mob} \approx 41 \pm 1°$, the limitation of strength placed on design ($\phi < 40$ º) by USFHWA and AASHTO seems both pragmatic and reasonable.
- The main implication of the durability assessment for current design practice is that isochronous load curves can be used with confidence for characterizing the long-term strains of uniaxial geogrid reinforcement.

6.5 Recommendations for future work

Based on the analysis of laboratory test data, and the companion back-analysis of the reinforced steep slope, the subsequent recommendations for future work are made:

- Recognizing that the testing of Skedsmo sand was performed at only one value of relative density, further testing at different values of relative density would be useful to fundamentally understand the behaviour of this sand at low stresses.
- Additional analysis of the reinforced structure, using the strength-strain curves obtained in the experimental study and a representative stress-strain soil model, would be useful to understand better the nature of strain compatibility within the structure, and thereby address a source of uncertainty in current design practice.
- It appears reasonable to use a peak friction angle for designing reinforced structures. Soil strength, especially in plane-strain conditions, is larger than expected, which could provide a candidate explanation for the small strains being measured in instrumented reinforced structures around the world: it is recommended that further effort be put into addressing this factor in other instrumented case studies.

REFERENCES

AASHTO (2009). LRFD Bridge Design Specifications, American Association of State Highway and Transportation Officials, 6th Edition, Washington, D.C.

Alabdullah, J. (2010). Testing unsaturated soil for plane strain conditions: a new double-wall biaxial device. PhD. Thesis. Bauhaus-University, Weimar, Germany.

Alshibli K. A., and H. S. Williams, (2005). A true triaxial apparatus for soil testing with mixed boundary conditions. *Geotechnical Testing Journal*, 28(6), 1-10.

ASTM Standard D698. (1942). Laboratory compaction characteristics of soil using standard effort (12 400 ft-lbf/ft3 (600 kN-m/m3)). ASTM International, West Conshohocken, PA.

Barden, L., Ismail, H., and Tong, P. (1969). Plane-strain deformation of granular material at low and high pressures. *Géotechnique*, 19(4), 441-452.

Berg, R.R., Christopher, B.R. and Samtani, N.C. (2009). Design of mechanically stabilized earth walls and reinforced soil slopes. Report FHWA-NHI-10-024, Federal Highway Administration (FHWA), Washington, D.C.

Bishop, A. W. (1966). The strength of soils as engineering materials. *Géotechnique*, 16(2), 91-130.

Bishop, A. W., and Henkel, D. J. (1978). The measurement of soil properties in the triaxial test. 4th ed. Edward Arnold Publishers Ltd., London, U.K.

Blight, G. E. (1963). The effect of nonuniform pore pressures on laboratory measurements of the shear strength of soils. Symposium, laboratory shear testing of soils, ASTM, S.T.P., Ottawa, 361.

Bolton, M.D. (1996). Geotechnical design of retaining walls, *The Structural Engineer*, 74(No. 21): 365-369.

Bolton, M. D. (1986). The strength and dilatancy of sands. *Géotechnique*, 36(1), 65-78.

Bolton, M.D. (1993). What are partial factors for? In Proc. International Symposium on Limit State Design in Geotechnical Engineering, Vol. Bulletin 10, pp. 565-583.

Boyle, S. R. (1995). Deformation prediction of geosynthetic reinforced soil retaining walls. PhD-Thesis. University of Washington, Seattle, US.

Bright, D.G., Collins, J.G., and Berg, R.R. (1994). Durability of geosynthetic soil reinforcement elements in Tanque Verde retaining wall structures, Transportation Research, Record 1439, ISSN: 0361-1981.

British Standard Institute (BSI). (2010). Code of practice for strengthened/reinforced soils and other fills. BS, 8006-1.

Campanella, R. G. and Vaid, Y.P. (1973). Influence of stress path on the plane strain behaviour of sensitive clay. *Proc. 8th Int. Conf. on Soil Mechanics and Foundation Engineering*, Moscow, U.S.S.R.

Cornforth, D. H. (1961). Plane strain failure characteristics of a saturated sand. PhD-Thesis. Imperial College, London.

Cornforth, D. H. (1964). Some experiments on the influence of strain conditions on the strength of sand. *Géotechnique*, 14(2), 143-166.

Desrues, J. (1984). La localisation de la déformation dans les matériaux granulaires. Thése de Doctorat es Science. USMG and INPG, Grenoble, France.

Duncan, J. M., and Seed, H. B. (1966). Strength variation along failure surfaces in clay. J*ournal of the Soil Mechanics and Foundations Division*, ASCE, 92(6), 81-104.

Elias, V. (2000). Long-term durability of geosynthetics based on exhumed samples from construction projects, US-Federal Highway Administration, Report FHWA-RD-00-157, NTIS PB2001-105580.

El-Nasrallah N.S. (1976). Shear strength of a cohesionless soil under plane strain and triaxial conditions. Master of Engineering Thesis, McMaster University, Hamilton Ontario. 104.

Fannin, R.J. (1988). An instrumented field study of the analysis and design of geogrid reinforced slope, Norwegian Geotechnical Institute, Oslo, Norway. Report 52757-10, 113 p.

Fannin, R.J. (1994). Field observations on the load-strain-time behavior of geogrid reinforcement, *Canadian Geotechnical Journal*, 31(4): 564 - 569.

Fannin, R.J. (2001). Long-term variations of force and strain in a steep geogrid reinforced soil slope, *Geosynthetics International*, 8(1): 81-96.

Fannin, R.J. and Hermann, S. (1990). Performance data for a sloped reinforced soil wall, *Canadian Geotechnical Journal*, 27(5): 676 - 686.

Finn, W. D. L., and Mittal, H. K. (1964). Laboratory shear testing of soils. *ASTM STP, American Society for Testing and Materials*, (361) 42-51.

Finno, R. J., Harris, W. W., and Viggiani, G. (1996). Strain Localization and Undrained Steady State of Sand. *Journal of Geotechnical Engineering*, 122(6) 462–473.

Finno, R. J., Harris, W. W., Mooney, M. A., and Viggiani, G. (1997). Shear bands in plane strain compression of loose sand, *Geotechnique*, 47 (1) 149–165.

Hanna, A. (2001). Determination of plane-strain shear strength of sand from the results of triaxial tests. *Canadian Geotechnical Journal*, (38) 1231-1240.

Harney, M. and Holtz, R.D. (2006). Mechanical properties of geotextile reinforcement, 30 years after installation, 8th International Conference on Geosynthetics, Yokohama, Japan, International Geosynthetics Society, 1041-1044.

Head, K. H. (1982). Manual of soil laboratory testing. Whittles Publishing. CRC Press

Jenner, C., and Nimmesgern, M. (2006). Geogrid reinforced railway embankment – excavation after ten years of loading, Geosynthetics State of the Art Recent Developments, Balkema, Rotterdam, Netherlands, 881-884.

Jewell, R.A. (1990). Revised design charts for steep reinforced slopes. In Proc. Symposium Reinforced Embankments: Theory and Practice in the British Isles, pp. 1-31.

Jewell, R.A. and Wroth, C.P. (1987). Direct shear tests on reinforced sand, *Géotechnique*, 37(1): 53-68.

Kjellman, W. (1936). Report on an apparatus for consummate investigation of the mechanical properties of soils. *Proceedings of the 1st International Conference on Soil Mechanics and Foundation Engineering*, (2) 16–20.

Knappett, J. A., and Craig, R. A. (2012). Craig's Soil Mechanics. Spon press, London &New York.

Krumbein, W.C. and Sloss, L.L. (1963). Stratigraphy and sedimentation. Freeman and Company, San Francisco.

Mitchell, R.J. (1973). An apparatus for plane strain and true triaxial testing of undisturbed soil samples. *Canadian Geotechnical Journal*. 10. p. 520

Ladd, R. S. (1978). Preparing tests specimens using undercompaction. *Geotechnical Testing Journal*, GTJODJ, 1(1), 16-23.

Lee, K. L., and Seed, H. B. (1967). Drained characteristics of sand. *Journal of Soil Mechanics and Foundations Division*, 93(6), 117-141.

Lehane, B. M., and Liu, Q. B. (2013). Measurement of shearing characteristics of granular materials at low stress levels in a shear box. *Geotechnical Geological Engineering*, 31 329-336.

Marachi, N. D., Duncan, J. M., Chan, C. K., and Seed, H. B. (1981). Plane strain testing of sand. Laboratory Shear Strength of Soil: A Symposium Sponsored by ASTM Committee D-18 on Soil and Rock for Engineering Purposes, *American Society for Testing and Materials*, West Conshohocken, Chicago, 294–302.

Oda, M. (1972). Initial fabrics and their relations to mechanical properties of granular material. *Soils and Foundations*, 12(1), 17-36.

Oda, M., Koshikawa, I., and Higuchi, T. (1978). Experimental study of anisotropic shear strength of sand by plane strain test. *Soils and Foundations*, 18(1), 25-38.

Onodera, S., Hirai, T., Hazama, A., and Itagaki, S. (2004). Long-term durability of geogrids laid in reinforced soil wall. Third Geosynthetics Conference, EuroGeo3, Munich, Germany.

Riemer, M. F. (1999). Plane strain testing of sand specimens for RMC test wall modeling. Test report. Berkeley, Calif. (unpublished).

Rowe, P. W. (1969). The relationship between the shear strength of sands in triaxial compression, plane strain and direct shear. *Géotechnique*, 19(1), 75-86.

Tsomokos, A. and Georgiannou, V.N. (2010). Effect of grain shape and angularity on the undrained response of fine sands, *Canadian Geotechnical Journal*, 47: 539–551.

Vaid, Y. P. (1968). A plane strain apparatus for soil. Master Thesis. University of British Columbia UBC, Vancouver, BC, Canada.

Vaid, Y. P., and Saivathayalan, S. (2000). Fundamental factors affecting liquefaction susceptibility of sands. *Canadian Geotechnical Journal*, 37 pp. 592– 606.

Vaid, Y. P., and Sasitharan, S. (1992). The strength and dilatancy of sand. *Canadian Geotechnical Journal*, 29 522-526.

Wanatowski, D. (2005). Strain softening and instability of sand under plane-strain conditions. PhD-Thesis. Nayang Technological University, Singapore.

Wayne, M., Bright, D., Berg, R.R., and Fishman, K. (1997). Tanque Verde retaining wall structure: revised after 11 years. *Geotextiles and Geomembranes*, 15(4-6): 223-233.

Wood, C. C. (1958). Shear strength and volume change characteristics of compacted soils under conditions of plane strain. PhD-Thesis. Univ. of London.